

ON THE INTERPLAY BETWEEN STAR FORMATION AND FEEDBACK IN GALAXY FORMATION SIMULATIONS

OSCAR AGERTZ^{1,2,3} AND ANDREY V. KRAVTSOV^{2,3,4}
ApJ submitted

ABSTRACT

Using high resolution cosmological zoom-in simulations of galaxy formation, we investigate the star formation-feedback cycle at high redshifts ($z > 1$), focusing on progenitors of Milky Way-sized galaxies. Our star formation model is based on the local density of molecular hydrogen (H_2) forming on dust grains, as this may be an important ingredient for regulating star formation in the high redshift, metal-poor regime of galaxy formation. Our stellar feedback model accounts for energy and momentum from supernovae, stellar winds and radiation pressure. We use a suite of simulations with different parameters and assumptions about star formation and prescription recipes. We find that in order to reproduce global properties of the Milky Way progenitors, such as star formation history and stellar mass-halo mass relation, simulations should include 1) a combination of local early ($t \lesssim 4$ Myr) momentum feedback via radiation pressure and stellar winds and subsequent efficient supernovae feedback, and 2) the global star formation efficiency on kiloparsec scales should be *feedback regulated*. In particular, we find that in models with efficient feedback, the *local* efficiency of star formation per free fall time can be substantially larger than the global star formation efficiency inferred from the Kennicutt-Schmidt relation. We find that simulations that adopt inefficient star formation inferred from such relation fail to produce vigorous outflows and eject sufficient amounts of enriched gas in order to regulate the galactic baryon content. This illustrates the importance of understanding the complex interplay between star formation and feedback and the detailed processes that contribute to the feedback-regulated formation of galaxies. Although we find that the results of galaxy formation simulations are quite sensitive to the implementation details of the star formation-feedback cycle, it is encouraging that our fiducial model provides a good match to all considered observables at $z \gtrsim 1$: semi-empirically derived star formation histories, the stellar mass-gas metallicity relation and evolution, the Kennicutt-Schmidt relation, the $M_* - M_{\text{halo}}$ relation and its evolution, as well as the flat shape of rotation curves.

Subject headings: cosmology: theory – galaxies: feedback – methods: numerical

1. INTRODUCTION

The basic scenario of hierarchical galaxy formation (White & Rees 1978; Fall & Efstathiou 1980) has been greatly elaborated and put on a firm footing within the Cold Dark Matter paradigm during the last three decades. Although the Λ Cold Dark Matter (Λ CDM) model has proven broadly successful in explaining and predicting a variety of observations, such as the Cosmic Microwave Background temperature anisotropies (e.g. Komatsu et al. 2011; Hinshaw et al. 2013; Planck Collaboration et al. 2013), evolution of cluster abundance (Vikhlinin et al. 2009), and large scale distribution of matter in the Universe (Conroy et al. 2006; Springel et al. 2006), many aspects of the theory of galaxy formation are not yet fully understood (see, e.g., Silk & Mamon 2012, for a recent review).

One of the most pressing problems in galaxy formation modelling is understanding why galaxies forming at the centers of dark matter halos are so inefficient in converting their baryons into stars. A number of different methods, such as dark matter halo abundance matching (Conroy & Wechsler 2009; Guo et al. 2010), satellite kinematics (Klypin & Prada 2009; More et al. 2011), and weak lensing (Mandelbaum et al. 2006) (see Kravtsov et al. 2014, for a comprehensive dis-

cussion) point towards *peak* stellar to dark matter mass fractions of $M_*/M_h \approx 3 - 5\%$ on average for L_* galaxies (e.g., Kravtsov et al. 2014), far below the cosmological baryon fraction $\Omega_b/\Omega_m \approx 16\%$ (Planck Collaboration et al. 2013).

The low galactic baryon fractions are believed to be due to galactic winds driven by stellar feedback at the faint end of the stellar mass function (Dekel & Silk 1986; Efstathiou 2000) and by the active galactic nuclei (AGN) and the bright end (Silk & Rees 1998; Benson et al. 2003). Modeling these processes in fully cosmological hydrodynamical simulations has proven to be a daunting task due to the multi-scale nature of galaxy formation, where properties of the intergalactic distribution of baryons, on scales $\gtrsim 100$ kpc, are affected by star formation and feedback processes on scales of individual star clusters ($\lesssim 1$ pc).

Although the formal spatial resolution $\sim 10 - 100$ pc, comparable to the scale of massive giant molecular clouds (GMCs), is not uncommon in modern cosmological galaxy formation simulations (e.g. Kravtsov 2003; Gnedin & Kravtsov 2010; Agertz et al. 2009; Hopkins et al. 2013), the relevant star formation and feedback processes remain “sub-grid”. In particular, substantial differences in resulting galaxies may arise when different implementations and parameterizations of these processes are used in simulations, even when the same initial conditions are used (Governato et al. 2010; Scannapieco et al. 2012).

Implementations of stellar feedback in galaxy formation simulations have been explored in many studies over the last two decades (e.g. Katz 1992; Navarro & White 1993; Katz et al. 1996; Thacker & Couchman 2001; Stinson et al. 2006;

¹ Department of Physics, University of Surrey, Guildford, GU2 7XH, United Kingdom o.agertz@surrey.ac.uk

² Department of Astronomy & Astrophysics, The University of Chicago, Chicago, IL 60637 USA

³ Kavli Institute for Cosmological Physics, The University of Chicago, Chicago, IL 60637 USA

⁴ Enrico Fermi Institute, The University of Chicago, Chicago, IL 60637 USA

Governato et al. 2007; Scannapieco et al. 2008; Colín et al. 2010; Agertz et al. 2011; Avila-Reese et al. 2011; Guedes et al. 2011; Scannapieco et al. 2012; Hopkins et al. 2011; Christensen et al. 2012; Brook et al. 2012; Stinson et al. 2013; Agertz et al. 2013; Ceverino et al. 2013; Roškar et al. 2013; Booth et al. 2013). Nevertheless, we still do not have a full understanding of what processes matter most for suppressing star formation and driving galactic winds over the vast range of observed galaxy masses.

Recent studies (Leitner 2012; Weinmann et al. 2012; Behroozi et al. 2013; Moster et al. 2013) have shown that not only is galaxy formation an inefficient process, but also that star formation in progenitors of most galaxies ($L \lesssim L_*$) is significantly suppressed during the first 3 Gyr of cosmic evolution. van Dokkum et al. (2013) recently reached a similar conclusion by matching cumulative co-moving number densities in the 3D-HST and CANDELS Treasury surveys, demonstrating that $\sim 90\%$ of the stellar mass in Milky Way mass galaxies formed after $z \sim 2.5$.

Much effort has gone into reproducing the $z = 0$ $M_* - M_h$ relation over a large range of galaxy masses in simulations with efficient feedback (e.g., Munshi et al. 2013). At the same time, predicting its evolution, and hence reproducing the significant suppression of star formation necessary at $z \gtrsim 2$ has proven more difficult. Brook et al. (2012) and Stinson et al. (2013) discussed the importance of “early feedback”⁵ in their SPH simulations, here modeled by assuming that 10% of the bolometric luminosity radiated by young stars get converted into thermal energy. This large energy injection resulted in star formation histories consistent with the data of Moster et al. (2013). Similar results were found by Aumer et al. (2013) who considered a momentum based model of radiation pressure, although with the value of the infrared optical depth of $\tau_{\text{IR}} \sim 25$, larger than in the models by Hopkins et al. (2011) and Agertz et al. (2013). Hopkins et al. (2013), Ceverino et al. (2013), and Trujillo-Gomez et al. (2013), also found that radiative feedback, both due to photoionization and radiation pressure, could play an important role in low mass galaxies (here progenitors of galaxies with $M_{\text{vir}}(z = 0) \lesssim 10^{12} M_{\odot}$) at high redshifts, even for more moderate values of photon trapping by dust.

While suppression of star formation in simulations of galaxy formation via strong stellar feedback has been widely explored in the recent literature, freedoms in the way in which star formation in the interstellar medium (ISM) is modeled has received less attention. Recent work by Gnedin et al. (2009, see also Gnedin & Kravtsov 2010, 2011; Kuhlen et al. 2012; Christensen et al. 2012) demonstrated how a star formation model based on the local abundance of H_2 could explain the observed steepening for $\Sigma_{\text{gas}} < 100 M_{\odot} \text{pc}^{-2}$ in the Kennicutt-Schmidt (KS) relation for $z \approx 3 - 4$ Damped Lyman- α systems and Lyman Break Galaxies (LBGs). Governato et al. (2010) found that a high threshold for star formation, in conjunction with higher resolution and strong feedback, can lead to more correlated feedback events and a more realistic halo baryon fraction. These results illustrate that it is paramount to explore how parameters of the star formation recipe and feedback implementation affect basic properties of galaxies forming in a given halo.

In this paper we present results of a systematic study of such dependencies using high resolution, cosmological simulations

⁵ Feedback that operates at times before the first SNe explosions, i.e. $t \lesssim 4 \text{ Myr}$, for a coeval stellar population.

of the Milky Way (MW) sized progenitors, that include implementation of our new model for stellar feedback described in Agertz et al. (2013). We specifically explore how the interplay between various modes of star formation and feedback models affect large scale galactic characteristics at $z \gtrsim 1$. The paper is organized as follows: In § 2 we outline our numerical method as well as star formation and feedback models. § 3 describes the initial conditions and the simulation suite. In § 4 and 5 we describe the simulation results, followed discussion and conclusions in § 6 and 7.

2. NUMERICAL CODE

We carry out cosmological hydro+ N -body simulations using the Adaptive Mesh Refinement (AMR) code RAMSES (Teyssier 2002). The fluid dynamics of baryons is calculated using second-order unsplit Godunov method, while collisionless dynamics of stellar and dark matter particles is evolved using the particle-mesh technique with gravitational accelerations computed from gravitational potential on the mesh. Gravitational potential is calculated by solving the Poisson equation using the multi-grid method (Brandt 1977) for all refinement levels. The potential is used to compute accelerations for both particles and baryon fluid. The equation of state of the fluid is that of an ideal mono-atomic gas with an adiabatic index $\gamma = 5/3$. The code achieves high resolution in high density regions using adaptive mesh refinement. The refinement strategy is based on a quasi-Lagrangian approach, in which the number of collisionless particles per mesh cell is kept approximately constant, which allows to match local force softening to the local mean interparticle separation and suppress discreteness effects (e.g., Knebe et al. 2000; Romeo et al. 2008).

2.1. Star formation

We model the local star formation rate using the following equation:

$$\dot{\rho}_* = f_{\text{H}_2} \frac{\rho_{\text{g}}}{t_{\text{SF}}}, \quad (1)$$

where f_{H_2} is the local H_2 mass fraction, ρ_{g} is the gas density in a cell, and t_{SF} is the star formation time scale of *molecular* gas. In § 2.3 we describe the model we use to calculate f_{H_2} . The time scale t_{SF} is defined by the efficiency of star formation, which, as we show below, is one of the key parameters controlling basic properties of galaxies forming in a given halo and efficacy of stellar feedback. Given its importance, we will discuss the empirical constraints and our choices for the value of this parameter in our simulations in § 2.2 below.

To ensure that the number of star particles formed during the course of a simulation is tractable, we sample Equation 1 stochastically at every fine simulation time step Δt (see section 2.3 in Agertz et al. 2013, for details). We also adopt a temperature threshold by only allowing star formation to occur in cells of $T < 10^4 \text{ K}$, although we find that this threshold has no actual impact on the resulting star formation rates.

By adopting a star formation relation of Eq. 1 we avoid imposing a fixed, and perhaps arbitrary, star formation density threshold, as is common in the galaxy formation community. We explore the difference between the constant density threshold approach and the molecular hydrogen based star formation model further Appendix A. As described in § 1, relating star formation to the molecular gas is well motivated empirically, as galactic star formation rate surface densities

correlate well with the surface density of molecular gas independent of metallicity, and poorly or not at all with the surface density of atomic gas measured on kpc scales (Bigiel et al. 2008; Krumholz et al. 2009b; Gnedin et al. 2009).

2.2. Efficiency of star formation

The star formation time scale of *molecular* gas, t_{SF} , in our star formation rate equation 1 is related to the efficiency of star formation in gas of a given density. Following Krumholz & Tan (2007) we can write this time scale as $t_{\text{SF}} = t_{\text{ff}}/\epsilon_{\text{ff}}$, where $t_{\text{ff}} = \sqrt{3\pi/32G\rho_{\text{g}}}$ is the local free-fall time of the gas and ϵ_{ff} is the star formation efficiency per free-fall time. As we show below, basic properties of galaxies forming in a given halo and the degree to which these properties are affected by stellar feedback depend sensitively on the value of t_{SF} or ϵ_{ff} . It is therefore important to discuss motivation for particular choices for the values of this parameter we make in our simulations.

Star formation overall, and the efficiency with which a given molecular region converts its gas mass into stars, are not yet fully understood theoretically. Nevertheless, useful empirical constraints do exist. Moreover, over the last decade robust theoretical models predicting star formation efficiency have also been developed.

On large, kiloparsec scales observational measurements show that the gas consumption time scale of molecular gas is $t_{\text{H}_2, \text{gal}} \approx 2$ Gyrs (Bigiel et al. 2008). If ϵ_{ff} had a universal value in all of the molecular gas, we would expect direct relation between the global molecular gas consumption time scale and $t_{\text{SF}} = t_{\text{H}_2, \text{gal}}$ and thus $\epsilon_{\text{ff}} = t_{\text{ff, SF}}/t_{\text{H}_2, \text{gal}}$. The typical free-fall time in GMCs, observed to be the sites of most star formation, is $\langle t_{\text{ff}} \rangle \approx 5 \times 10^6$ years, as can be seen in Figure 1. In this figure we show the free-fall time for individual GMCs in the samples in both the Milky Way and other galaxies collected from the literature, as described in the caption. For each GMC, t_{ff} was computed as $t_{\text{ff}} = \sqrt{3\pi/32G\rho_{\text{GMC}}}$, where $\rho_{\text{GMC}} = 3M_{\text{GMC}}/(4\pi R^3)$ is the mean density of GMC computed using its mass and density reported in the corresponding sample.

The figure shows that $t_{\text{ff, GMC}}$ does not depend on GMC mass. The median value is $t \sim 5 \times 10^6$ yrs, but the scatter in individual values is quite large with values spanning the range from $\approx 10^6$ to 3×10^7 years. These values imply the values of ϵ_{ff} from 0.0005 to 0.015, with median of ≈ 0.0025 . The long global consumption time scale of the molecular gas, thus, implies very low star formation efficiencies in star forming gas.

These values of ϵ_{ff} are significantly lower, however, than estimates for individual star forming regions that are typically found to be several times larger and span the range of $\epsilon_{\text{ff, SF}} \sim 0.01 - 0.1$ (Lada et al. 2010; Murray 2011; Evans et al. 2014). This is illustrated in Figure 2, which shows values of ϵ_{ff} estimated for samples of GMCs in the Milky Way by Murray et al. (2011) and Evans et al. (2014) as a function of GMC mass. We have also included GMCs analyzed by Lada et al. (2010) for which we have estimated ϵ_{ff} assuming a fixed free-fall time of 5×10^6 yrs corresponding to the median free-fall time of GMCs in Figure 1.

Note that numerical simulations of turbulent bound star forming clouds (e.g., see Padoan et al. 2013, for a recent review) also generally predict values of ϵ_{ff} much larger than 0.0025. Such theoretical predictions may thus explain the high values of ϵ_{ff} in a fraction of the most bound, massive

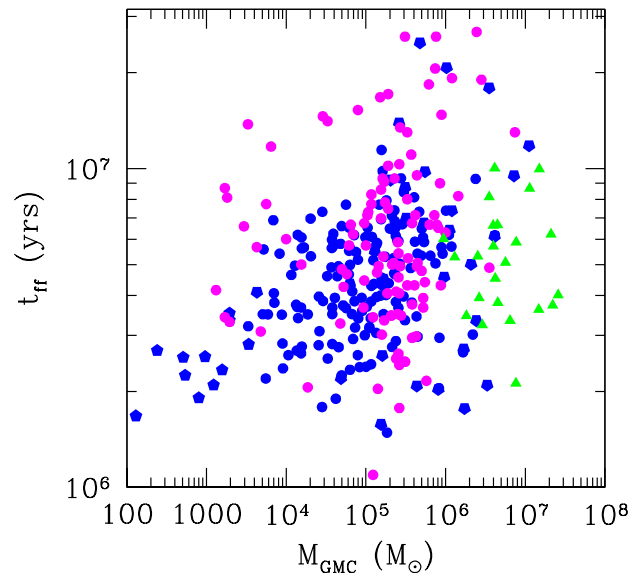


FIG. 1.— Mean free-fall time of giant molecular clouds in different samples and galaxies. *Blue circles* show GMCs from the sample of Heyer et al. (2009), *blue pentagons* are GMCs presented in Table 1 of Murray (2011), *magenta circles* show GMCs in several nearby galaxies including the Milky Way from the sample of Bolatto et al. (2008), and *green triangles* show GMCs in dense molecular inner region of M64 in the sample of Rosolowsky & Blitz (2005).

GMCs.

The sizeable difference in values of ϵ_{ff} derived from the global molecular gas consumption time scale and direct estimates in star forming clouds indicates that significant fraction of molecular gas is not star forming or forms stars with extremely low efficiency. This is corroborated by the measurement of molecular gas consumption time scale distribution of molecular gas in patches of 12 pc radius in the SMC by Bolatto et al. (2011). The typical consumption time scale for molecular gas is indeed several billion years and high star formation efficiency is reached only in a small fraction of molecular patches.

These considerations indicate that value of ϵ_{ff} in star forming regions on small scales does not have to correspond to the global value implied by the molecular gas consumption time scale on kiloparsec scales and can be significantly larger. In our study we therefore consider a range of values of ϵ_{ff} from 0.01 to 0.1.

2.3. Molecular hydrogen model

Krumholz et al. (2008), Krumholz et al. (2009a), and McKee & Krumholz (2010) developed a model for the abundance of H_2 based on radiative transfer calculations of idealized spherical giant atomic–molecular complexes subject to a uniform and isotropic Lyman-Werner (LW) radiation field. When the H_2 abundance is calculated assuming formation-dissociation balance, the solution can conveniently be expressed as

$$f_{\text{H}_2} \simeq 1 - \frac{3}{4} \frac{s}{1 + 0.25s}, \quad (2)$$

$$s = \frac{\ln(1 + 0.6\chi + 0.01\chi^2)}{0.6\tau_c}, \quad (3)$$

TABLE 1
LIST OF COSMOLOGICAL ZOOM-IN SIMULATIONS. ALL SIMULATIONS REACH A MINIMUM CELL SIZE OF $\Delta x = 75$ PC.

Simulation	Description
<i>KMT09 models</i>	
NoFB_e001	No feedback (only metal enrichment), $\epsilon_{\text{ff}} = 1\%$
NoFB_e010	No feedback (only metal enrichment), $\epsilon_{\text{ff}} = 10\%$
ALL_e010	All feedback processes, $\epsilon_{\text{ff}} = 10\%$
<i>KMT09 models, feedback energy variable E_{fb}, $f_{\text{fb}} = 0.5$, $t_{\text{dis}} = 10$ Myr</i>	
ALL_Efb_e010	All feedback processes, $\epsilon_{\text{ff}} = 10\%$
NoPrad_Efb_e010	All feedback processes but radiation pressure, $\epsilon_{\text{ff}} = 10\%$
ALL_Efb_e001	All feedback processes, $\epsilon_{\text{ff}} = 1\%$
ALL_Efb_e001_5ESN	All feedback processes, $E_{\text{SNII}} = 5 \times 10^{51}$ erg, $\epsilon_{\text{ff}} = 1\%$
<i>Fixed threshold for star formation ($n_* = 25 \text{ cm}^{-3}$), E_{fb}, $f_{\text{fb}} = 0.5$, $t_{\text{dis}} = 10$ Myr</i>	
ALL_Efb_e010_n25 (see appendix A)	All feedback processes, $\epsilon_{\text{ff}} = 10\%$

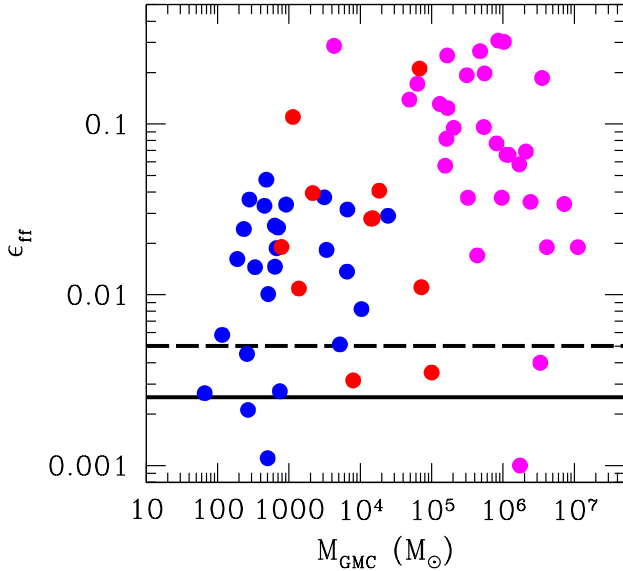


FIG. 2.— Efficiency per free-fall time for giant molecular clouds in the samples of Evans et al. (2014, blue points), Lada et al. (2010, red points) and Murray et al. (2011, magenta points). The solid line shows the value of ϵ_{ff} implied by the median global molecular gas consumption scale of $\tau_{\text{H}_2} = 2$ Gyrs inferred from the Kennicutt-Schmidt relation Bigiel et al. (2008), while the dashed line shows similar estimate from the $\tau_{\text{H}_2} \approx 1$ Gyr estimate specifically for the Milky Way.

$$\chi = 71 \left(\frac{\sigma_{d,-21}}{\mathcal{R}_{-16.5}} \right) \frac{G'_0}{n_{\text{H}}}, \quad (4)$$

where τ_c is the dust optical depth of the cloud, $\sigma_{d,-21}$ is the dust cross-section per hydrogen nucleus to radiation at 1000 Å normalized to 10^{-21} cm^2 and n_{H} is the volume density of hydrogen nuclei in units of cm^{-3} . The coefficient $\mathcal{R}_{-16.5}$ is the rate for H_2 formation on dust grains, normalized to the Milky Way value of $10^{-16.5} \text{ cm}^3 \text{ s}^{-1}$ (see Wolfire et al. 2008) and G'_0 is the ambient UV radiation field intensity, normalized to the Draine (1978) value for the Milky Way. As both σ_d

and \mathcal{R} are linearly proportional to the dust abundance, and hence gas metallicity, their ratio in χ becomes independent of metallicity.

The equations above can be simplified further by assuming pressure equilibrium between the cold and warm neutral medium (CNM and WNM respectively). Krumholz et al. (2009a) demonstrated that the assumption of pressure balance between the two gas phases causes the minimum CNM density to be linearly proportional to the UV radiation field:

$$n_{\text{min}} \approx \frac{31}{1 + 3.1 Z_{\text{g}}^{0.365}} G'_0, \quad (5)$$

where Z_{g} is the gas metallicity in units of solar metallicity, $Z_{\odot} = 0.020$. By allowing for the CNM density to be larger than the minimum density by a factor ϕ_{CNM} , i.e. $n_{\text{H}} = \phi_{\text{CNM}} n_{\text{min}}$, Eq. 4 becomes

$$\chi = 2.3 \left(\frac{\sigma_{d,-21}}{\mathcal{R}_{-16.5}} \right) \frac{1 + 3.1 Z_{\text{g}}^{0.365}}{\phi_{\text{CNM}}}. \quad (6)$$

As seen in the equation above, the molecular hydrogen mass fraction becomes independent of the local LW intensity. Krumholz & Gnedin (2011) found that the two phase approximation predicts the H_2 abundance accurately compared to full non-equilibrium radiative transfer calculations for $Z_{\text{g}} \gtrsim 10^{-2} Z_{\odot}$.

In the remainder of the paper we refer to the above model, including the two-phase CNM-WNM equilibrium assumption, as the KMT09 model. The KMT09 model was adopted in fully cosmological simulations of galaxy formation by Kuhlen et al. (2012) and Kuhlen et al. (2013), who demonstrated how the model led to a strong suppression of star formation in low-mass halos ($M_{\text{h}} \lesssim 10^{10} M_{\odot}$) at $z > 4$, in agreement with galaxy formation simulations of Gnedin & Kravtsov (2010) which used full non-equilibrium calculations of H_2 abundance.

2.4. Feedback

The stellar feedback model adopted in our simulations is described in detail in Agertz et al. (2013). Briefly, each formed stellar particle is treated as a single-age stellar population with a Chabrier (2003) initial mass function (IMF).

Several processes are contributing to stellar feedback, as stars inject energy, momentum, mass and heavy elements over time via SNII and SNIa explosions, stellar winds and radiation pressure on the surrounding gas. Hence, at every simulation time step, and for every stellar particle, we account for the following energy, momentum, mass loss and metal injection rates

$$\begin{aligned}
 \text{Energy:} \quad \dot{E}_{\text{tot}} &= \dot{E}_{\text{SNII}} + \dot{E}_{\text{SNIa}} + \dot{E}_{\text{wind}} \\
 \text{Momentum:} \quad \dot{p}_{\text{tot}} &= \dot{p}_{\text{SNII}} + \dot{p}_{\text{wind}} + \dot{p}_{\text{rad}} \\
 \text{Mass loss:} \quad \dot{m}_{\text{tot}} &= \dot{m}_{\text{SNII}} + \dot{m}_{\text{SNIa}} + \dot{m}_{\text{wind}} + \dot{m}_{\text{loss}} \\
 \text{Metals:} \quad \dot{m}_{\text{Z,tot}} &= \dot{m}_{\text{Z,SNII}} + \dot{m}_{\text{Z,SNIa}} + \dot{m}_{\text{Z,wind}} + \dot{m}_{\text{Z,loss}},
 \end{aligned} \tag{7}$$

Each term in the above equations depends on the stellar age, mass and gas/stellar metallicity, all accounted for and described in Agertz et al. (2013). Feedback is thus not done instantaneously, but continuously at the appropriate times when the various feedback processes are known to operate, taking into account the lifetime of stars of different masses in a stellar population. To track the lifetimes of stars within the population we adopt the metallicity dependent age-mass relation of Raiteri et al. (1996).

The effect of radiation pressure is modeled as a direct injection of momentum to the cells surrounding newly formed star particles. Here the momentum injection rate from radiation can be written as

$$\dot{p}_{\text{rad}} = (\eta_1 + \eta_2 \tau_{\text{IR}}) \frac{L(t)}{c}, \tag{8}$$

where τ_{IR} is the infrared optical depth and $L(t)$ is the luminosity of the stellar population, here taken from the stellar evolution code `STARBURST99` (Leitherer et al. 1999). The first term describes the direct radiation absorption/scattering, and given the large dust and HI opacities in UV present in dense star forming regions, $\eta_1 \approx 1$. The second term describes momentum transferred by infrared photons re-radiated by dust particles, and scattered multiple times by dust grains before they escape, where η_2 is added to scale the fiducial value of τ_{IR} . As cosmological simulations cannot resolve the density structure around young massive star clusters on sub-parsec scales, to estimate τ_{IR} we use the empirically-motivated sub-grid model described in Agertz et al. (2013).

The momentum due to stellar winds, radiation pressure, and SN blastwaves is added to the 26 nearest cells surrounding parent cell of the stellar particle. The thermal energy due to SNe and shocked stellar winds is injected directly into the parent cell.

In most of our simulations we explore the concept of retaining some fraction of the thermal feedback energy in a *separate* gas energy variable over longer times than expected purely from the local gas cooling time scale. This approach was discussed by Agertz et al. (2013), and previously by Teyssier et al. (2013), and can be viewed as accounting for the effective pressure from a multiphase medium, where local unresolved pockets of hot gas exert work on the surrounding cold phase, or a placeholder for other sources of energy, such as turbulence and cosmic rays (Booth et al. 2013).

As described in section 3.2 of Agertz et al. (2013), at each time step Δt we inject a fraction f_{fb} of the calculated feedback energy into a separate energy variable, E_{fb} , and the remaining energy fraction, $1 - f_{\text{fb}}$, is released as thermal energy into the main energy variable. E_{fb} has units of energy per unit volume

and evolves according to the following equation⁶:

$$\frac{\partial}{\partial t} (E_{\text{fb}}) + \nabla \cdot (E_{\text{fb}} v_{\text{gas}}) = -P_{\text{fb}} \nabla \cdot v_{\text{gas}} - \frac{E_{\text{fb}}}{t_{\text{dis}}}. \tag{9}$$

The feedback energy is thus continuously dissipated over a time-scale t_{dis} , i.e. $E_{\text{fb}}^{t+\Delta t} = E_{\text{fb}}^t \exp(-\Delta t/t_{\text{dis}})$. We make the assumption that the dissipation timescale is comparable to the decay time of supersonic turbulence, which is of order of the flow crossing time (Ostriker et al. 2001). In all of the simulations presented in this paper, we adopt a fixed $t_{\text{dis}} = 10$ Myr, typical for a few crossing times in massive GMCs ($l \sim 10 - 100$ pc), or the vertical crossing time in cold galactic disks, with characteristic velocity dispersions $\sigma_{\text{HI}} \sim 10 \text{ km s}^{-1}$.

Heavy elements (metals) injected by supernovae and winds are advected as a passive scalar and are incorporated self-consistently in the cooling and heating routine. The code takes into account metallicity dependence of the cooling by using tabulated cooling functions of Sutherland & Dopita (1993) for cooling at temperatures $10^4 - 10^{8.5}$ K, which is extended cooling down to $T = 300$ K using rates from Rosen & Bregman (1995). Heating from the UV background (UVB) radiation is accounted using the UVB model of Haardt & Madau (1996) assuming reionization redshift of $z = 8.5$. We follow Agertz et al. (2009) and adopt an initial metallicity of $Z = 10^{-3} Z_{\odot}$ in the high-resolution region (see §3) in order to account for enrichment from unresolved Pop III star formation (e.g. Wise et al. 2012).

3. INITIAL CONDITIONS AND SIMULATION SUITE

The initial conditions used in this work are identical to those presented in Agertz et al. (2011). In summary, we adopt a *WMAP5* (Komatsu et al. 2009) compatible Λ CDM cosmology with $\Omega_{\Lambda} = 0.73$, $\Omega_{\text{m}} = 0.27$, $\Omega_{\text{b}} = 0.045$, $\sigma_8 = 0.8$ and $H_0 = 70 \text{ km s}^{-1} \text{ Mpc}^{-1}$. A pure dark matter simulation was performed using a simulation cube of size $L_{\text{box}} = 179 \text{ Mpc}$. At $z = 0$, a halo of mass $M_{200c} \approx 9.7 \times 10^{11} M_{\odot}$ was selected for re-simulation at high resolution, and traced back to the initial redshift of $z = 133$. Here M_{200c} is defined as the mass enclosed within a sphere with mean density 200 times the critical density at the redshift of analysis. The corresponding radius is $r_{200c} = 205 \text{ kpc}$. The mass within the radius enclosing overdensity of 200 times the mean density is $M_{200m} = 1.25 \times 10^{12} M_{\odot}$ and $r_{200m} = 340 \text{ kpc}$. When baryons are included in the simulations, the final *total* halo mass remains approximately the same.

The selected halo does not experience any major merger after $z = 1$, favouring the formation of an extended late-type galaxy. A nested hierarchy of initial conditions for the dark matter and baryons was generated using the `GRAFIC++`⁷ code, where we allow for the high resolution particles to extend to three virial radii from the centre of the halo at $z = 0$. This avoids mixing of dark matter particles with different masses in the inner parts of the domain. The dark matter particle mass in the high resolution region is $m_{\text{DM}} = 3.2 \times 10^5 M_{\odot}$ and the adaptive mesh is allowed to refine if a cell contains more than eight dark matter particles, and similar criterion is employed for the baryonic component. At the maximum level

⁶ note that this differs from the original implementation in Agertz et al. (2013) who neglected the $-P_{\text{fb}} \nabla \cdot v$ term. In Agertz et al. (2013), the adiabatic cooling via $p dV$ work done by the *total* pressure was affecting only the thermal energy component.

⁷ <http://grafic.sourceforge.net/>

of refinement, the simulations reach a physical resolution of $\Delta x \approx 75$ pc.

3.1. Simulation suite

The main focus of this work is to investigate the interplay between star formation and feedback. To this end, we carry out a suite of simulations targeting a number of different regimes; 1) no stellar feedback from young stars, 2) all sources of stellar feedback are operating (as discussed in § 2.4), 3) the impact of neglecting radiative feedback and 4) the impact of making SN energy feedback less efficient by not tracking it as a separate fluid variable.

For the first two regimes we also study the impact of varying the efficiency of star formation per-free-fall time (see § 2.1) using simulations with $\epsilon_{\text{ff}} = 1\%$ and 10% . The lower efficiency is closer to the value derived from the gas consumption time scale in kpc-sized patches of the ISM (see § 2.2 above). However, the relevant values of ϵ_{ff} for GMCs as a function of environment is not fully understood, as we discussed above in § 2.2 (see Fig. 2). Simulating galaxy formation using larger efficiency of $\epsilon_{\text{ff}} = 10\%$ is thus motivated by GMC observations and allows us to study the ability for stellar feedback to regulate the *measured* efficiency to globally observed values.

Our fiducial simulations include all feedback process discussed above, including the second energy variable and star formation efficiency of $\epsilon_{\text{ff}} = 10\%$. For the case of $\epsilon_{\text{ff}} = 1\%$, we also investigate the effect of increasing the available feedback energy from SNII events, going from the fiducial $E_{\text{SNII}} = 10^{51}$ erg to $5 \times E_{\text{SNII}}$. Such increase could correspond for a somewhat more top heavy IMF.

In Appendix A we compare results of our simulations with H_2 based star formation with similar simulation in which star formation is assumed to proceed at densities above a fixed density threshold. For the latter simulation we adopt density threshold of $n_* = 25 \text{ cm}^{-3}$, which roughly corresponds to the physical density at which $f_{\text{H}_2} \sim 50\%$ at $Z_g = Z_\odot$. We note that this threshold value is larger than the value adopted in the Eris simulation (Guedes et al. 2011), where $n_* = 5 \text{ cm}^{-3}$ was used, although close to the $n_* = 20 \text{ cm}^{-3}$ adopted for the followup Eris2 simulation.

The entire simulation suite, and the associated star formation and feedback parameters, are summarized in Table 1.

4. RESULTS

In this section we present a detailed analysis of a number of basic galaxy properties at $z \gtrsim 1$, relevant for star forming Milky Way analogues, that ought to be reproduced by simulations of galaxy formation: the star formation history, the stellar mass-dark matter halo mass ($M_* - M_{\text{vir}}$) relation, the Kennicutt-Schmidt ($\Sigma_{\text{gas}} - \Sigma_{\text{SFR}}$) relation and the stellar mass-gas metallicity ($M_* - Z_{\text{gas}}$) relation. Furthermore, we study the ability of our models to predict rising or flat rotation curves, a key ingredient to explain the observed Tully-Fisher relation (galaxy luminosity vs. disk circular velocity, Tully & Fisher 1977) for extended spiral galaxies (Reyes et al. 2012).

4.1. A qualitative comparison

In Fig. 3 we show large scale maps of the gas surface density, mass weighted temperature, gas metallicity and stellar surface density, at $z = 3$, for four of our simulations: ALL_Efb_e010, ALL_Efb_e001, ALL_Efb_e001_5ESN and ALL_e010 (see table 1). From

the first two simulations, which *only* differ in their choice of star formation efficiency per free fall time, we find a dramatic difference in outflow properties; for $\epsilon_{\text{ff}} = 10\%$, galactic winds eject enriched gas from the turbulent galactic disk, while no signs of outflows can be seen when $\epsilon_{\text{ff}} = 1\%$. In the latter case, almost all metals are retained in the cold star forming gas disk, which is also the case for simulations neglecting feedback. The stellar distribution in this simulation is also significantly more compact compared to other runs, in which feedback drives significant outflows.

Furthermore, the size of the hot gaseous halo surrounding the main progenitor differs between the simulations; in models with inefficient or no feedback, the hot halo forms via cosmological accretion shocks or shocks generated via rapid gravitational potential fluctuations. At $r \sim 50$ kpc, which is close to the virial radius at this redshift, the temperature drops off to $T < 10^5$ K. In contrast, in simulations with strong feedback-driven winds, the gas outflows contribute significantly to pressurizing the hot halo and driving the outer shock. The hot ($T \gtrsim 10^6$ K) halo in such simulations extends far beyond the virial radius of the main dark matter halo.

Boosting the feedback energy per supernova by a factor of five for the case of $\epsilon_{\text{ff}} = 1\%$ radically changes the mode of galaxy formation, and similar metal enriched outflows and turbulent gas disk morphology as for our fiducial simulations is recovered, at least qualitatively. This shows that there is a certain degeneracy between the star formation efficiency and feedback strength, and a quantitative comparison with observations may be necessary to separate the models.

We find that specific sources of stellar feedback matter and neglecting them leads to significant differences in galaxy evolution. For example, in the simulation shown in the rightmost column of Fig. 3 we do not include the second feedback energy variable, E_{fb} , while keeping the rest of the parameters the same as in our fiducial simulation (the leftmost panel). While metal rich outflows are still present, the gaseous disk is significantly less turbulent and is more compact, with less neutral gas extending to large distances (~ 10 kpc in the fiducial run), as seen in the temperature map. This results in a more massive stellar system, which as we demonstrate below is in tension with semi-empirically derived stellar mass-halo mass relations (Behroozi et al. 2013). A similar conclusion holds for the simulations that neglect radiation pressure.

4.2. Star formation histories

Figure 4 shows the star formation histories (SFHs), calculated in bins of $\Delta t = 100 \text{ Myr}$ ⁸, for the simulated galaxies compared to the semi-empirically inferred SFH from Behroozi et al. (2013) relevant for a galaxy forming in a $M_{\text{vir}}(z=0) = 10^{12} M_\odot$ dark matter halo. Regardless of the choice of star formation efficiency per free fall time, neglecting feedback leads to a dramatic overestimate of galactic SFR at all redshifts by $\gtrsim 1$ dex compared to the predictions by Behroozi et al.. This may seem counterintuitive as the lower abundance of H_2 in dwarf galaxies at high redshifts is thought to make star formation less efficient. However, as the ISM self-enriches via SNe, and no stellar feedback is present to drive metal rich winds, a larger fraction of the

⁸ Note that the degree of fluctuations in star formation rate is sensitive to the choice of Δt_{SF} and can vary with stellar mass, as reported by Hopkins et al. (2013) (see also Feldmann et al. 2012). The scatter in our simulated galaxy increases towards higher redshift as star formation is found to be highly episodic in the low mass progenitors ($M_{\text{vir}} < 10^{11} M_\odot$).

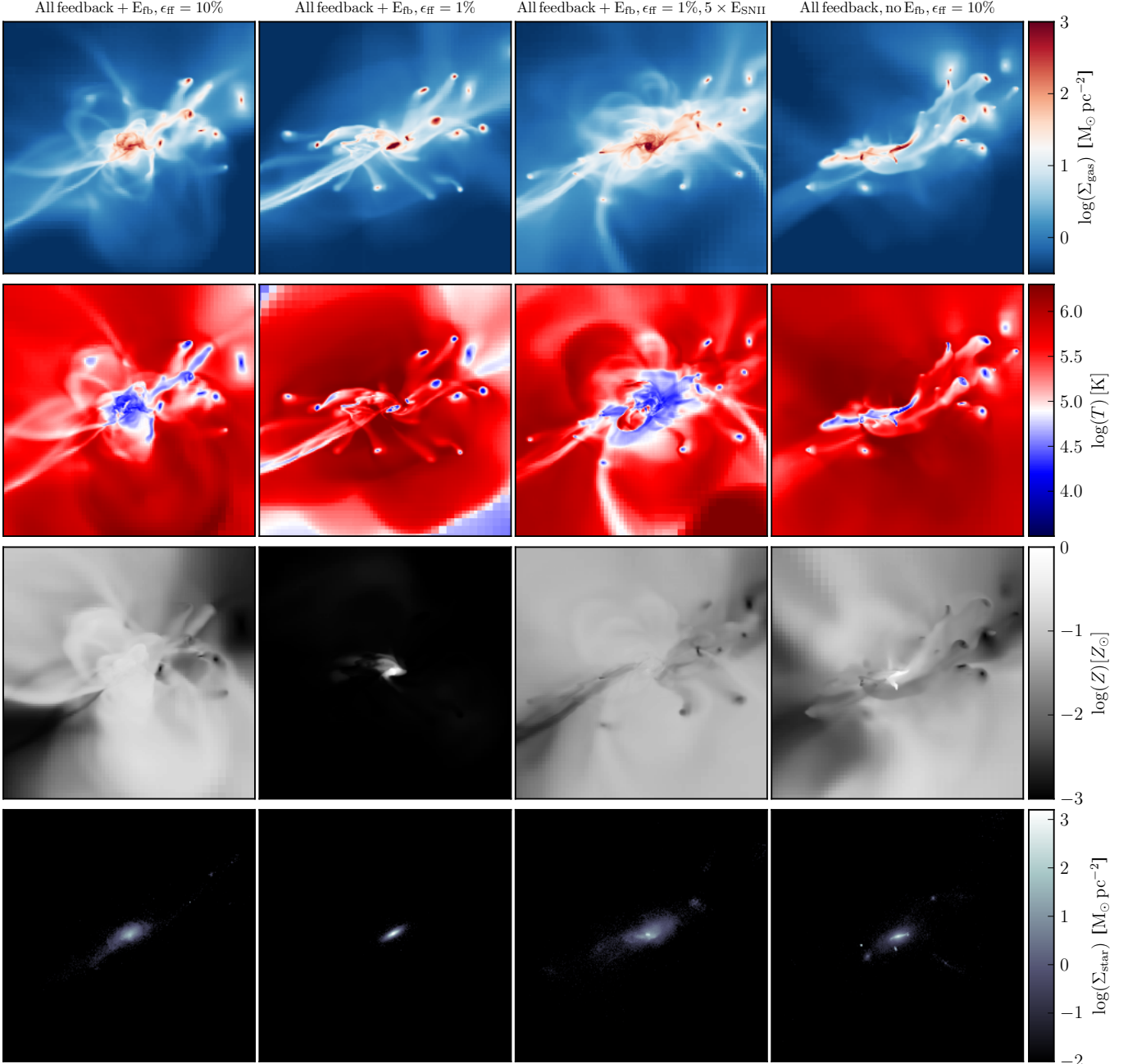


FIG. 3.— Maps of, from top to bottom, gas surface density, mass weighted temperature, gas metallicity and stellar surface density stellar for, from left to right, ALL_Efb_e010, ALL_Efb_e001, ALL_Efb_e001_5ESN and ALL_e010 at $z = 3$. The maps show regions 90 kpc on each side. All simulations, apart from ALL_Efb_e001, show clear signatures of outflows. As discussed in the text, the low input free-fall time efficiency of star formation ($\epsilon_{\text{ff}} = 1\%$) does not allow for local feedback to be vigorous enough to generate galactic winds.

gas mass rapidly becomes available for star formation due to the effectively lower density threshold via the higher f_{H_2} , see § 2.3. As mentioned above, this is the case regardless of the adopted value for ϵ_{ff} , although the normalization of the relation at $z > 4$, and hence how rapidly the galaxy self-enriches, depends on the precise value.

Simply incorporating efficient stellar feedback (§ 2.4) in the KMT09 model does not necessarily overcome this problem. The simulation with $\epsilon_{\text{ff}} = 1\%$ overpredicts the SFRs by up to a factor of ten and the star formation rate in this case is not significantly affected by feedback. For star formation to be suffi-

ciently feedback regulated, the local star formation efficiency per free fall time needs to be sufficiently large: $\epsilon_{\text{ff}} = 10\%$. Once this is satisfied, the simulations are in excellent agreement with the data of Behroozi et al. (2013). In a star formation model based on H_2 abundance model, such as KMT09, the gas metallicity plays an important role in setting the fraction of gas available for star formation. The local metallicity, in turn, is regulated by the feedback driven outflows. In our current simulation suite, this only occurs if star formation, and hence feedback, becomes sufficiently spatially and temporally correlated. As we show in § 4.4, the simulations with efficient

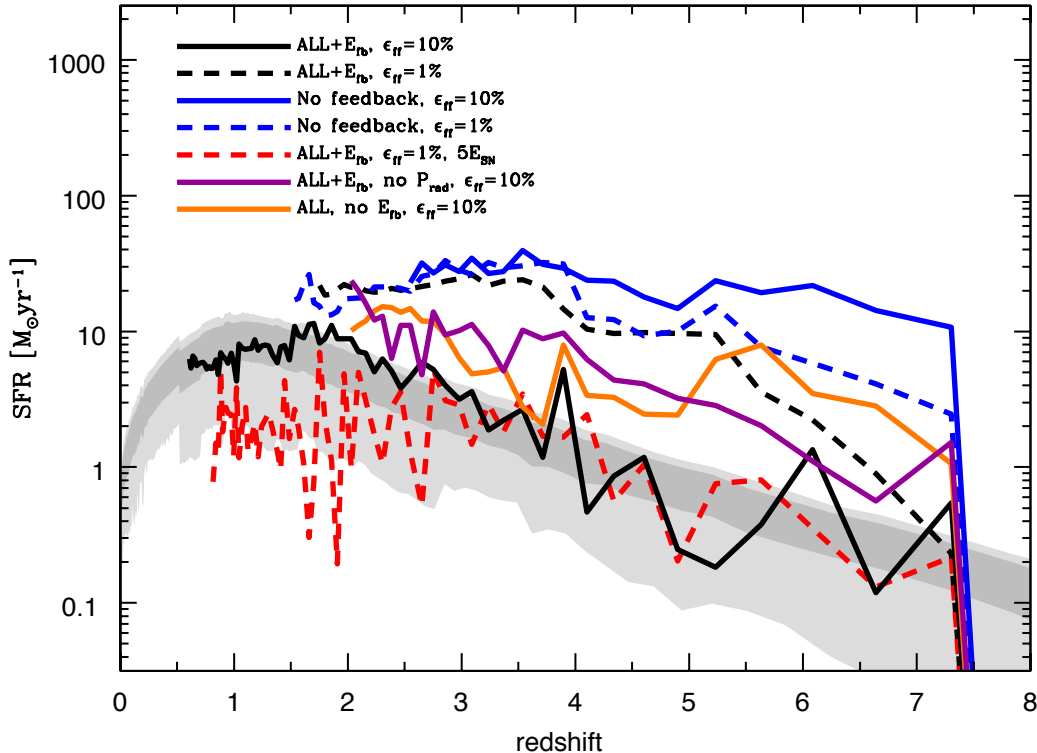


FIG. 4.— Simulated star formation histories compared to the Behroozi et al. (2013) data for $M_{\text{vir}}(z=0) = 10^{12} M_{\odot}$. Dark and light gray shaded areas are one- and two-sigma confidence regions respectively. We adopt bins of size $\Delta t_{\text{SF}} = 100 \text{ Myr}$ for the simulated SFHs. Without feedback, SFRs are overpredicted by at least one order of magnitude at $z > 1$. Efficient feedback in conjunction with $\epsilon_{\text{ff}} \gtrsim 10\%$ (ALL_Efb_e010) renders a star formation history in agreement with the Behroozi et al. data. In simulations with low star formation efficiency of $\epsilon_{\text{ff}} = 1\%$, the effectiveness of feedback diminishes and SFRs is ~ 1 dex higher than expected. Boosting the available SNe feedback (ALL_Efb_e001_5ESN) alleviates this, but leads to a significantly stronger suppression of star formation at $z \lesssim 2.5$. Both radiation pressure and efficient SN feedback appear crucial, as removing any of these feedback sources offsets the SFH by up to ~ 1 dex, as discussed in the text.

wind driving also match the observed evolution of the relation between stellar mass and gas metallicity.

Star formation suppression can also be achieved by increasing the available SN thermal energy budget, here illustrated by employing a boost by a factor of five for the run with $\epsilon_{\text{ff}} = 1\%$. The resulting SFH agrees almost perfectly with the less energetic, but self-regulated, fiducial simulation at $z \gtrsim 3$. As discussed in § 4.1, this illustrates a certain degeneracy between details of star formation and feedback prescriptions in such simulations, which needs to be broken by other observables, especially because the feedback boosted simulation severely distorts the gas disk at $z < 2$, as seen in Fig. 9.

In Fig. 4 we also show the impact of neglecting various sources of stellar feedback in our fiducial simulation. By not considering radiation pressure feedback, star formation rates increase by a factor of several at all redshifts, as found in Agertz et al. (2013) for isolated disks. Reducing the efficiency of thermal feedback, by neglecting the feedback energy variable, significantly increases the SFRs at $z > 4$, while bringing them into agreement with the Behroozi data at later times. This behavior stems from the inability of radiative feedback to efficiently regulate star formation in low metallicity gas at high redshifts, as photon trapping via dust becomes negligible, whereas this is not the case in the more enriched disk at late times. This collective, and highly non-linear behavior of early radiative feedback and SNe was recently studied in a fully cosmological setting by Hopkins et al. (2013), who also found that it was necessary to consider these two feedback processes jointly in order to reproduce observationally

derived star formation histories.

4.3. The stellar mass-halo mass relation

In Figure 5 we show the stellar mass fraction (M_*/M_h) vs. halo mass relation for the simulated galaxies. The shaded regions show the inferred 2σ relations for $z = 3, 2, 1$, from Behroozi et al. (2013). For consistency with Behroozi et al. (2013), we use the virial mass definition of Bryan & Norman (1998) to define the halo mass of the progenitor. The M_*/M_h evolutionary tracks are shown for all simulations for $z \gtrsim 1$, wherever simulation data exists. We note that the M_*/M_h relation on occasion rapidly evolves vertically, or that M_h even decreases temporarily. This behavior stems from major merger events which not only boosts star formation, but can complicate measurements of the halo virial mass.

Note that the M_*/M_h relation and SFHs in the previous section are not independent constraints. Indeed, simulations that also match the inferred SFHs in the previous section are in good agreement with the predicted stellar mass fractions, i.e. runs employing $\epsilon_{\text{ff}} = 10\%$ and/or efficient feedback (ALL_Efb_e010 and ALL_Efb_e001_5ESN). Inefficient local star formation ($\epsilon_{\text{ff}} = 1\%$) overpredicts the stellar content by an order of magnitude, while in runs in which feedback is neglected the stellar fraction is close to the mean cosmic baryon fraction at all times.

The interplay between radiation pressure and efficient thermal feedback in establishing a realistic stellar mass fraction is illustrated whenever either one of these sources is removed from the feedback budget; the stellar fraction is suppressed to

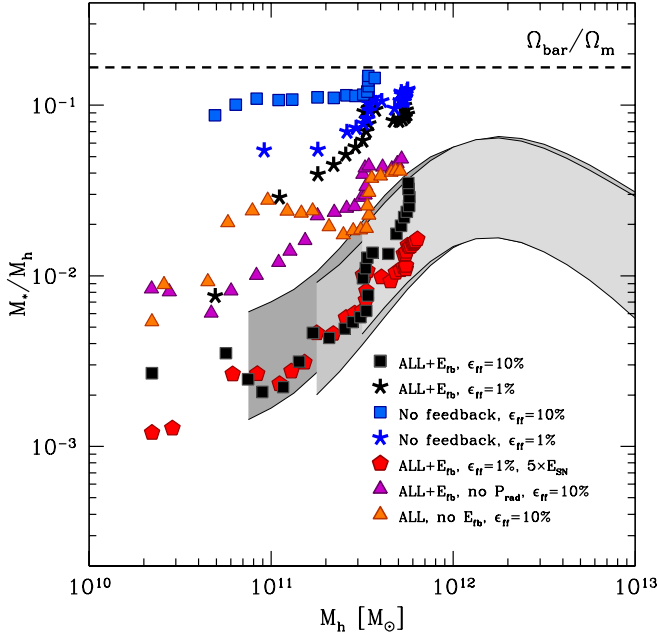


FIG. 5.— The evolution of the stellar mass fraction as a function of halo mass. The shaded regions show, from dark to light grey, the $z = 3, 2$ and 1 data from Behroozi et al. (2013) where the thickness encompasses $\pm 2\sigma$. The dashed horizontal line shows the average cosmic baryon fraction for the adopted cosmology. The simulated data points span the galactic growth from $z = 1-7$. As concluded for the star formation histories in Fig. 4, the simulations adopting efficient feedback and star formation (ALL_Efb_e010), as well as boosted SNe feedback (ALL_Efb_e001_5ESN) are in good agreement with the semi-empirical relation of Behroozi et al. Removing individual feedback source, or feedback altogether, offsets the simulated data by $\gtrsim 1$ dex from the average relation.

a much greater degree at late times (i.e. more massive dark matter halos) when E_{fb} is neglected, and the opposite is true when radiation pressure is neglected.

4.4. The mass-metallicity relation and effective yields

Fig. 6 shows the stellar mass-gas metallicity ($M_* - Z_{gas}$) relation for the simulated galaxies at $z = 2-2.5$ and $z = 3-4$. We compare the simulations with observational data of galaxies at $z \sim 0.1$ (Tremonti et al. 2004; Kewley & Ellison 2008), $z \sim 2.2$ (Erb et al. 2006) and $z \sim 3.5$ (Maiolino et al. 2008). In order to compare data to the observational aperture adopted by Maiolino et al. (2008), we quantify the gas metallicity as the mass weighted mean metallicity at radii $r \leq 3$ kpc. The stellar mass is the total stellar mass for $r \leq 10$ kpc, which safely contains all stellar mass belonging to the central galaxies at all redshifts under investigation. As we only track the average metallicity of the gas in RAMSES, we calculate $12 + \log(O/H)$ assuming solar mixture and adopt $12 + \log(O/H)_{\odot} = 8.69$ for the solar value (Asplund et al. 2009).

From Fig. 6 we find that *not* matching the SFH, M_*/M_{halo} and KS relations in the previous sections may still allow the galaxy to conform to the observed $M_* - Z_{gas}$ relation at $z > 3$. In fact, the almost 2 dex spread in stellar mass ($8.5 < M_* < 10.5$) in the simulation suite measured at $z = 3-4$ forms a steeper linear relation, $12 + \log(O/H) \approx 7.5 + \log(M_*/10^9 M_{\odot})$. Individual simulations, e.g. the favoured ALL_Efb_e010 run, traces a more shallow relation over the same redshift range. When $\epsilon_{ff} = 1\%$ (ALL_Efb_e001), or no feedback is present, star formation is not efficiently reg-

ulated leading to increasing stellar masses and metallicities that eventually causes the galactic average to diverge from the mean relation at lower redshifts. At $z = 2$, these particular simulations are already roughly in agreement with the $z \sim 0$ relation, but in strong disagreement with $z \sim 2-2.5$ data of Erb et al. (2006). The fiducial simulation (ALL_Efb_e010) is in excellent agreement with observations at all times. In the case of boosted SNe feedback energy (ALL_Efb_e001_5ESN), gas metallicities are lower at all redshifts, possibly in tension with observed gas metallicities at $z \sim 2-2.5$, although at the low stellar masses under consideration ($M_* \sim 3 \times 10^9 M_{\odot}$) the metallicity measurements are only upper limits.

Even though neglecting radiation pressure overestimates stellar masses, see § 4.3, the enrichment history allows the galaxy to evolve "along" the evolving $M_* - Z_{gas}$ relation. This is not the case when the second feedback energy variable E_{fb} is neglected, as the metal rich gas disk can be seen to evolve off the observed relation already at $z \sim 4$, illustrating the need in our current models for efficient thermal feedback to regulate the galactic metal content.

4.4.1. Effective yields

To better understand the role of metal rich outflows, we calculate effective yield, defined as

$$y_{\text{eff}} = \frac{Z_{\text{gas}}}{\ln(1/f_{\text{gas}})}, \quad (10)$$

where $f_{\text{gas}} = M_{\text{gas}}/(M_{\text{gas}} + M_*)$ is the fraction of baryons in the gas phase. The effective yield has been widely used as a diagnostic of the evolution of the baryonic component of galaxies, and more specifically as a test of the validity of the closed-box approximation (Pagel & Patchett 1975; Edmunds 1990). Observationally, the effective yield is known to decrease with galactic mass (Tremonti et al. 2004), with a sharp decline around the mass of dwarf galaxies ($v_{\text{rot}} \lesssim 100 \text{ km s}^{-1}$, Garnett 2002).

Under the closed-box assumption, the effective yield is always equal to the true yield y_{true} , typically defined, for a single stellar population, as the mass in newly synthesized metals returned to the ISM normalized to the stellar mass of this population locked up in stellar remnants and long-lived stars, i.e.

$$y_{\text{true,rem}} = \frac{1}{1-R} \int_{0.1}^{100} m p_{\text{im}} \phi(m) dm, \quad (11)$$

where m is the stellar mass, $\phi(m)$ the IMF, p_{im} is the instantaneous stellar yield, and R the mass fraction returned to the ISM. For our feedback prescription we calculate the true yield, as well as the initial true yield, $y_{\text{true,ini}}$, where we consider $R = 0$, i.e. the stellar population is assumed to retain all of its initial birth mass.

Following Tassis et al. (2008), we calculate the "observed" effective yield as a function of total baryons mass in our main galaxy using Eq. 10, where we consider only the cold gas ($T \leq 10^4$ K) and the metal content within the stellar extent defined as the radius that includes 90% of the total stellar mass. The result for the entire simulations suite, over the redshift range $z = 1-7$, is presented in Fig. 7. Our fiducial simulation (ALL_Efb_e010) shows a clear plateau towards the true yield for $M_{\text{bar}} \gtrsim 10^{10} M_{\odot}$, with lower yields signifying outflows, as seen in the metal rich winds in Fig. 3. The same is true for the feedback boosted simulations, although

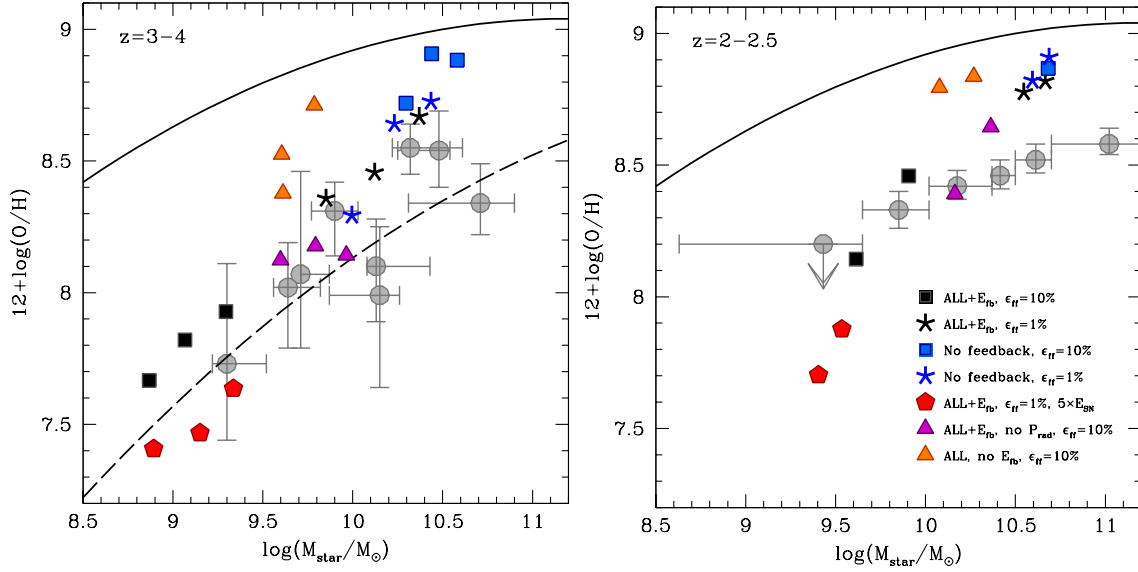


FIG. 6.— The stellar mass-gas metallicity relation at $z = 3-4$ (left) and $z = 2-2.5$ (right). (Left) Grey symbols show observational data from Maiolino et al. (2008) for individual galaxies at $z \sim 3.5$ where the lower dashed line is a fit to the data. The upper solid line shows the results of a re-analysis of the Tremonti et al. (2004) ($z \sim 0.1$) study by Kewley & Ellison (2008). When star formation is feedback regulated, the simulations conform with the observed $M_* - Z_{\text{gas}}$ relation. Without any feedback, or in the case of low star formation efficiency (ALL_Efb_e001), the galaxy rapidly evolves to a relation more akin to what is observed for $z \sim 0$ galaxies. When the available supernovae feedback energy is boosted by a factor of 5, the metal content stays lower than for the other runs (for the same stellar mass). (Right) Grey symbols here show observational data as presented in Erb et al. (2006) for galaxies at $z = 2.26 \pm 0.17$. We again find that simulations with efficient star formation regulation agrees with observational data, whereas a low star formation efficiency or no feedback results in metallicities closer to the observed $z = 0$ relation.

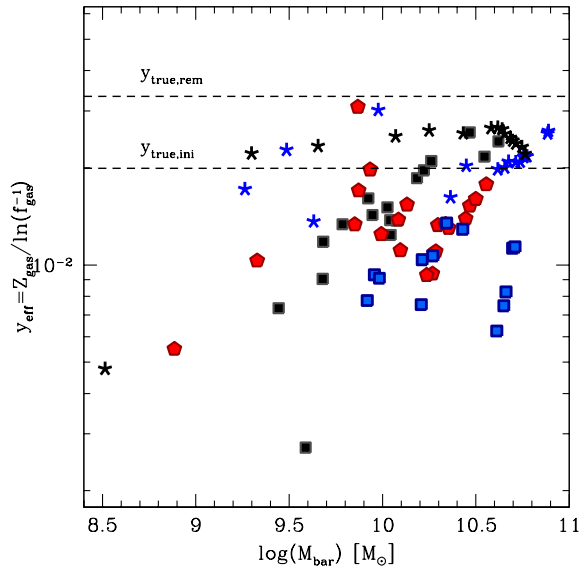


FIG. 7.— Effective yields for the main progenitor at $z = 1-8$ in the simulation suite. The data points are the same as in Fig. 6. A global trend is found for all galaxies to have yields lower than the expected true yields from a closed box model, but not necessarily for the same reason. The fiducial ALL_Efb_e010 simulations shows a clear evolution from low yields ($y_{\text{eff}} < 10^{-2}$), due to metal rich outflows, to a state where $y_{\text{eff}} \sim y_{\text{true}}$ for $M_{\text{bar}} \gtrsim 10^{10} M_{\odot}$. We refer to the main text for a detailed discussion.

the average values for $M_{\text{bar}} \gtrsim 10^{10} M_{\odot}$ are lower than for the fiducial case, indicating that outflows are still prominent.

Simulations with a low star formation efficiency, ALL_Efb_e001 and NoFB_e001, show effective yields close to the true yield already at early times, although the former simulation is significantly offset at $z \gtrsim 6$

($\log(M_{\text{bar}}) = 8.5$), indicating that the "observed" effective yield may not solely be explained via galactic winds (Tassis et al. 2008).

A peculiar result is found for the simulation without feedback and $\epsilon_{\text{ff}} = 10\%$ (NoFB_e010), which is shown for $2.5 < z < 7$. The effective yields lie significantly below all other data for $M_{\text{bar}} \gtrsim 10^{10} M_{\odot}$, despite having no means of ejecting enriched gas. The reason for this is that, despite being enriched to $Z_{\text{gas}} > Z_{\odot}$ already at early times, the gas fraction is kept very low due to the short depletion time-scale and low effective density threshold for star formation via the KMT09 model. In ALL_Efb_e010, $f_{\text{gas}}(r < 10 \text{ kpc}) \sim 65\%$ at $z = 2.5$, compared to $f_{\text{gas}} \sim 9\%$ for NoFB_e010, which pushes y_{eff} to lower values in the latter simulation.

4.5. Circular velocities

Simulated galaxies have traditionally displayed high central concentrations of baryons, leading to strongly peaked circular velocities towards the galactic center (Navarro & White 1993; Abadi et al. 2003; Okamoto et al. 2005; Scannapieco et al. 2009; Piontek & Steinmetz 2009; Hummels & Bryan 2012). Removal of preferentially low angular momentum gas via stellar feedback can remedy this problem (e.g. Governato et al. 2007; Agertz et al. 2011; Brook et al. 2012), hence bringing simulated galaxies closer to the observed Tully-Fisher relation (Tully & Fisher 1977; Pizagno et al. 2007).

Fig. 8 shows circular velocities of the entire suite of models in Table 1 adopting the KMT09 model at $z = 4, 3$ and 2. Strongly peaked circular velocities are found already at $z = 4$ for all models with no feedback, or where the star formation efficiency is too low ($\epsilon_{\text{ff}} = 1\%$) to allow for efficient wind driving. Adopting efficient feedback and efficient local star formation, as in our fiducial run (ALL_Efb_e010), as well as boosting the available SNe energy

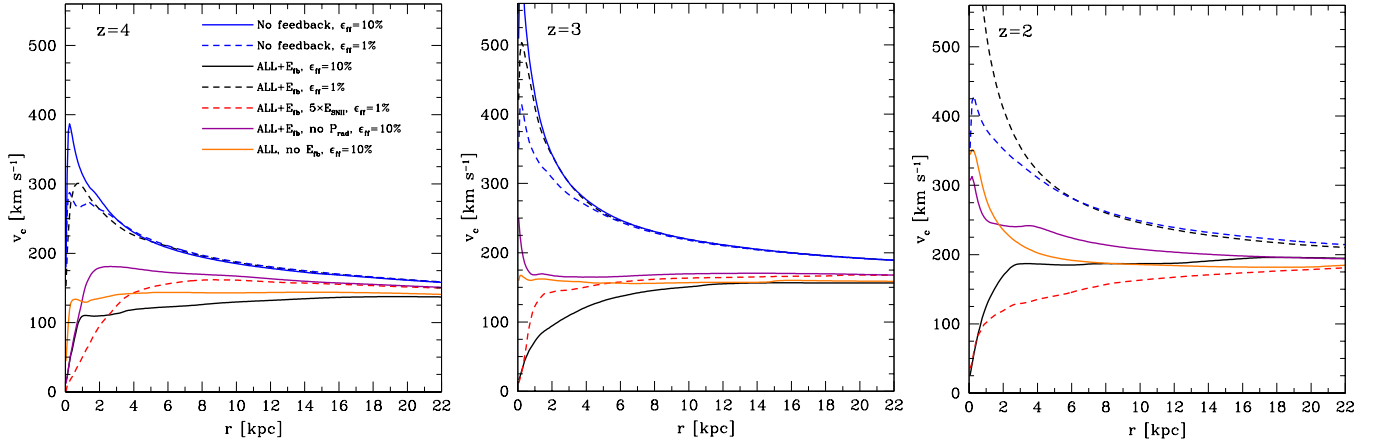


FIG. 8.— Circular velocities for the entire simulation suite at $z = 4$ (left), $z = 3$ (middle) and $z = 2$ (right). The only two simulations that maintain a rising or flat circular velocity profile are the fiducial simulation (ALL_Efb_e010) and the boosted SNe feedback run (ALL_Efb_e001_5ESN). As argued in the main text, only these two simulations regulate the star formation rates to reasonable levels while driving galactic winds. When radiation pressure or efficient thermal feedback is removed, the resulting rotation curves remain flat until $z \sim 3$, after which inefficient removal of low angular momentum material a significant upturn in circular velocities in the central parts of the galaxies.

(ALL_Efb_e001_5ESN), lead to a rising or flat rotation curve at all times due to efficient removal of low angular momentum gas in feedback driven outflows. Neglecting either radiation pressure or efficient thermal feedback via E_{fb} results in a massive bulge component at $z \lesssim 2$, demonstrating their important interplay in establishing galactic properties.

5. BREAKING THE DEGENERACY

As we have demonstrated in the previous section, the best matches to observations are found for two of our models: ALL_Efb_e010 and ALL_Efb_e001_5ESN. Both models of galaxy formation are able to reproduce global galactic characteristics, despite the significantly different star efficiency values and amount of feedback energy. To break this degeneracy, other properties of simulated galaxies need to be considered. Potentially, this can include a variety of observations, including studies of the circum-galactic medium (CGM), absorption lines studies of multiphase gas in the galactic halo, detailed properties of galactic winds etc. For now, we will study the morphological state of the main galaxy progenitor at lower redshifts, as well as internal star formation properties, here the $\Sigma_{\text{gas}} - \Sigma_{\text{SFR}}$ (Kennicutt-Schmidt) relation.

Fig. 9 shows the main galaxy progenitors in ALL_Efb_e010 and ALL_Efb_e001_5ESN at $z = 1$. At this epoch, the fiducial simulation has transitioned into a quiescent state of star formation, with a prominent (turbulent) gaseous disk in place, as well as an emerging stellar disk where stars form in cold clouds in transient spiral arm-like features, as observed e.g. in the Hubble Ultra Deep Field at $1 < z < 2$ (Elmegreen & Elmegreen 2014). This indicates that the disk may have entered an epoch of “disk settling”, as seen in the DEEP2 Survey (Kassin et al. 2012) for galaxies of stellar mass $8.0 < \log M_*(M_\odot) < 10.7$ over $0.2 < z < 1.2$. We detect individual hot super bubbles from correlated feedback events in the extended disk, leading to galactic outflows of enriched gas. Most of this enriched gas is found to enter a galactic fountain, rather than large scale outflows as seen at higher redshifts ($z > 2$). The gas disk metallicity at the redshift shown in the figure is close to solar.

The boosted feedback necessary to regulate the rate of star formation in the ALL_Efb_e001_5ESN simulation pro-

duces a significantly more turbulent system, with metals being spread over greater distances in comparison to the fiducial run. The cold gas metallicity in the central disk is also much lower, $Z_{\text{gas}} \sim 0.1 - 0.2 Z_\odot$. The strong feedback hinders the formation of a thin gas disk, indicating a striking difference in galaxy evolution compared to our fiducial model. A similar result was found by Agertz et al. (2011) and Roškar et al. (2013), where increasing the strength of feedback led to reasonable global characteristics at the cost of destroying the galactic disk.

5.1. The $\Sigma_{\text{gas}} - \Sigma_{\text{SFR}}$ relation

In Fig. 10 we plot the $\Sigma_{\text{gas}} - \Sigma_{\text{SFR}}$ -relation (the Kennicutt-Schmidt (KS) relation) at $z = 2 - 3$ for the entire simulation suite. We consider only the surface density of cold ($T \leq 10^4$ K) atomic and molecular gas, and do not include any contribution from helium⁹. We calculate Σ_{gas} and Σ_{SFR} in patches with an area $A = 750 \times 750 \text{ pc}^2$ evenly distributed across the simulated disks. We define $\Sigma_{\text{SFR}} \equiv m_* t_*^{-1} A^{-1}$ and consider the total mass of young stars m_* formed within $t_* = 20 \text{ Myr}$. For each galaxy and redshift we bin the resulting relation for Σ_{gas} in logarithmic bin sizes of 0.15 dex, and each panel contains measurements of simulations snapshots in the redshift range $z = 2 - 3$ at expansion factor intervals $\Delta a = 0.01$.

We compare the simulated relation to the KS relation inferred from observations of $z \sim 1 - 3$ normal star-forming galaxies from Genzel et al. (2010), $z \sim 3$ Damped Ly- α Systems (DLAs, Wolfe & Chen 2006), $z \sim 3$ low surface brightness emission around Lyman break galaxies (LBGs, Rafelski et al. 2011) as well as the relation of Kennicutt (1998) for $z \approx 0$ galaxies. Our simulated galaxy is hosted by halo of mass $M_h \sim \text{few} \times 10^{11} M_\odot$ at $z \sim 3$, which is consistent recent constraints from the cross-correlation between DLAs and Ly α forest that indicate that most DLAs at $z \approx 2 - 3$ are hosted by relatively massive halos (Font-Ribera et al. 2012). At $2 < z < 4$ DLAs are observed to have a wide distribution of metallicities, $\log(Z_{\text{gas}}) \sim -2.5$ to -0.5 , with a peak around $\log(Z_{\text{gas}}) \sim -1.5$ (Prochaska et al. 2007). Numerically

⁹ to scale our quoted surface densities to account for helium, multiply them by a factor of 1.36.

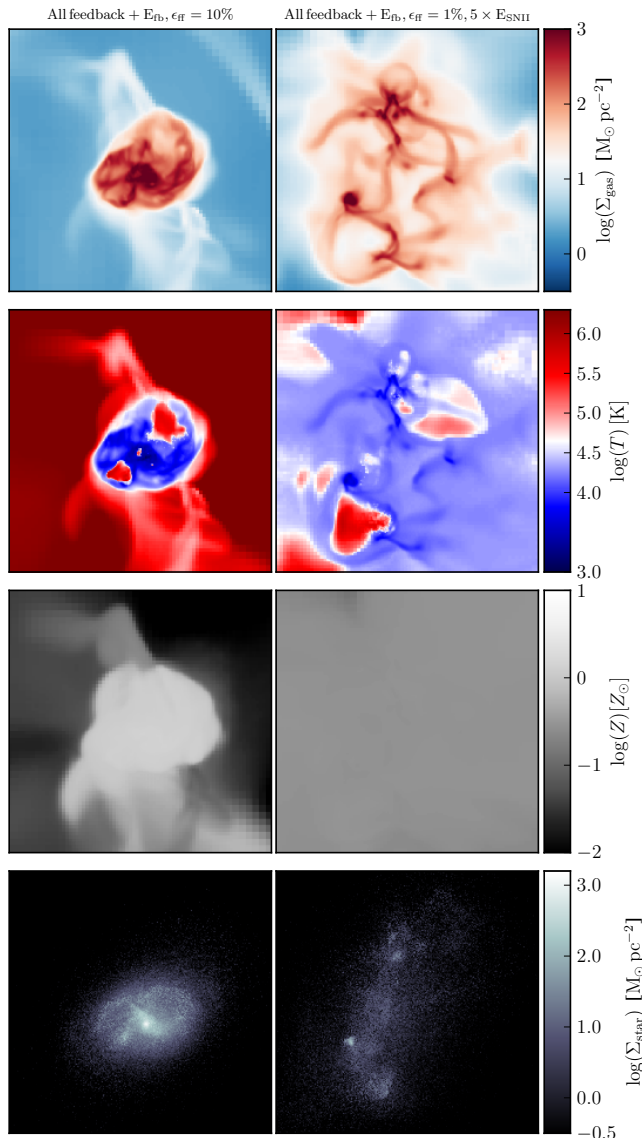


FIG. 9.— Maps of, from top to bottom, gas surface density, mass weighted temperature, gas metallicity and stellar surface density stellar for, from left to right, the fiducial ALL_Efb_e010 run and ALL_Efb_e001_5ESN, both at $z = 1$. The maps span 30 kpc on each side. As detailed in the text, both simulations compare favorably to the observed $\Sigma_{\text{gas}} - \Sigma_{\text{SFR}}$ relation, the stellar mass-gas metallicity relation ($M_* - Z_{\text{gas}}$), and the stellar mass-dark matter halo mass ($M_* - M_{\text{vir}}$) relation. However, the galactic morphologies are dramatically different; whereas the galaxy in fiducial simulation run eventually settles into an extended disk at the peak of star formation ($1 < z < 2$), the simulation adopting boosted SNe feedback, and a low star formation efficiency per free fall time, produces a heavily distorted gas distribution with a dispersion dominated stellar component. This illustrates the importance of the specific choices in modelling star formation and stellar feedback in shaping the resulting galaxy morphology.

cal models by Pontzen et al. (2008) have indicated that the metal rich DLAs are likely to be associated with halos of mass $M \gtrsim 10^{10} M_{\odot}$.

The KS relation for the MW progenitor galaxy in the fiducial simulation (ALL_Efb_e010) shown in the top left panel of Fig. 10 is in agreement with the empirical KS relation at $\Sigma_{\text{gas}} \gtrsim 100 M_{\odot} \text{pc}^{-2}$, and shows a clear drop below this surface density. This transition surface density is related to the physical density at which molecular hydrogen can be synthesized

on dust grains (Schaye 2001; Gnedin et al. 2009; Krumholz et al. 2009a; Gnedin & Kravtsov 2010, 2011). The lower star formation efficiency below this transition surface density, where the simulations match the DLA and LBG data, arises from the low gas metallicity, $Z_{\text{g}} \sim 0.1 - 0.2 Z_{\odot}$, in the outer disk which in turn results in a low f_{H_2} .

The KS relation in the simulation with $\epsilon_{\text{ff}} = 10\%$ (ALL_Efb_e010) is hence in very good agreement with observed KS relation of both low- z and high- z galaxies. Note that simulations with identical ingredients, but with $\epsilon_{\text{ff}} = 1\%$ (ALL_Efb_e001), is also consistent with observations at high surface densities but exhibits a drop in star formation at a somewhat larger gas surface density. The fact that the normalization of the KS relation is similar in simulations with a *local* efficiency of star formation different by a factor of ten illustrates that in simulations with efficient feedback and significant outflows, the normalization of the KS relation does not reflect the local star formation efficiency. In this case, the global star formation rate self-regulates to produce low overall star formation efficiency (i.e., long gas consumption time scale).

In contrast, in simulations in which feedback is weak or absent, the normalization of the KS relation is linearly related to the local efficiency. Thus, for example, the normalization in the simulation with $\epsilon_{\text{ff}} = 10\%$, but feedback turned off, is approximately an order of magnitude larger than that in the simulation with $\epsilon_{\text{ff}} = 1\%$ at $\Sigma_{\text{gas}} \gtrsim 100 M_{\odot} \text{pc}^{-2}$.

Figure 10 shows that the simulation with $\epsilon_{\text{ff}} = 1\%$ but the SN energy output boosted by a factor of five (ALL_Efb_e001_5ESN) has significantly lower normalization of the KS relation compared to our fiducial simulation and in tension with observations. As demonstrated more quantitatively in §4.4, this arises due to the very efficient removal of metal rich gas from the galaxy, leaving the entire disk metal poor with an outer disk metallicity $Z_{\text{g}} < 0.1 Z_{\odot}$. The marked difference between the internal star formation properties of ALL_Efb_e010 and ALL_Efb_e001_5ESN, which both conform to all observed *global* galactic characteristics, illustrates that it is potentially possible to break the degeneracy between such models using additional properties and observations.

6. DISCUSSION

6.1. Comparison with previous recent studies

A wide range of numerical studies of galaxy formation focusing on different stellar feedback processes have appeared in the past several years. It is thus useful to discuss how these models differ from, or agree with, the numerical models presented in this work and why.

Recently, Hopkins et al. (2013) presented a series of high-resolution cosmological zoom-in smoothed particle hydrodynamics (SPH) simulations of galaxy formation run to $z = 0$, spanning halo masses $M_{\text{halo}} \sim 10^8 - 10^{13} M_{\odot}$. Our results generally agree with those of Hopkins et al., who also find that star formation efficiency tends to self-regulate in the regime when stellar feedback is efficient. In particular, they found that the observed low normalization of the KS relation was reproduced in their simulations even when a local star formation efficiency as high as $\epsilon_{\text{ff}} = 100\%$ was used. Furthermore, Hopkins et al. (2013) also conclude that both early radiative feedback and subsequent supernova feedback are important. For the latter they use a scheme that allows to capture momentum generated during the unresolved Sedov-Taylor stage

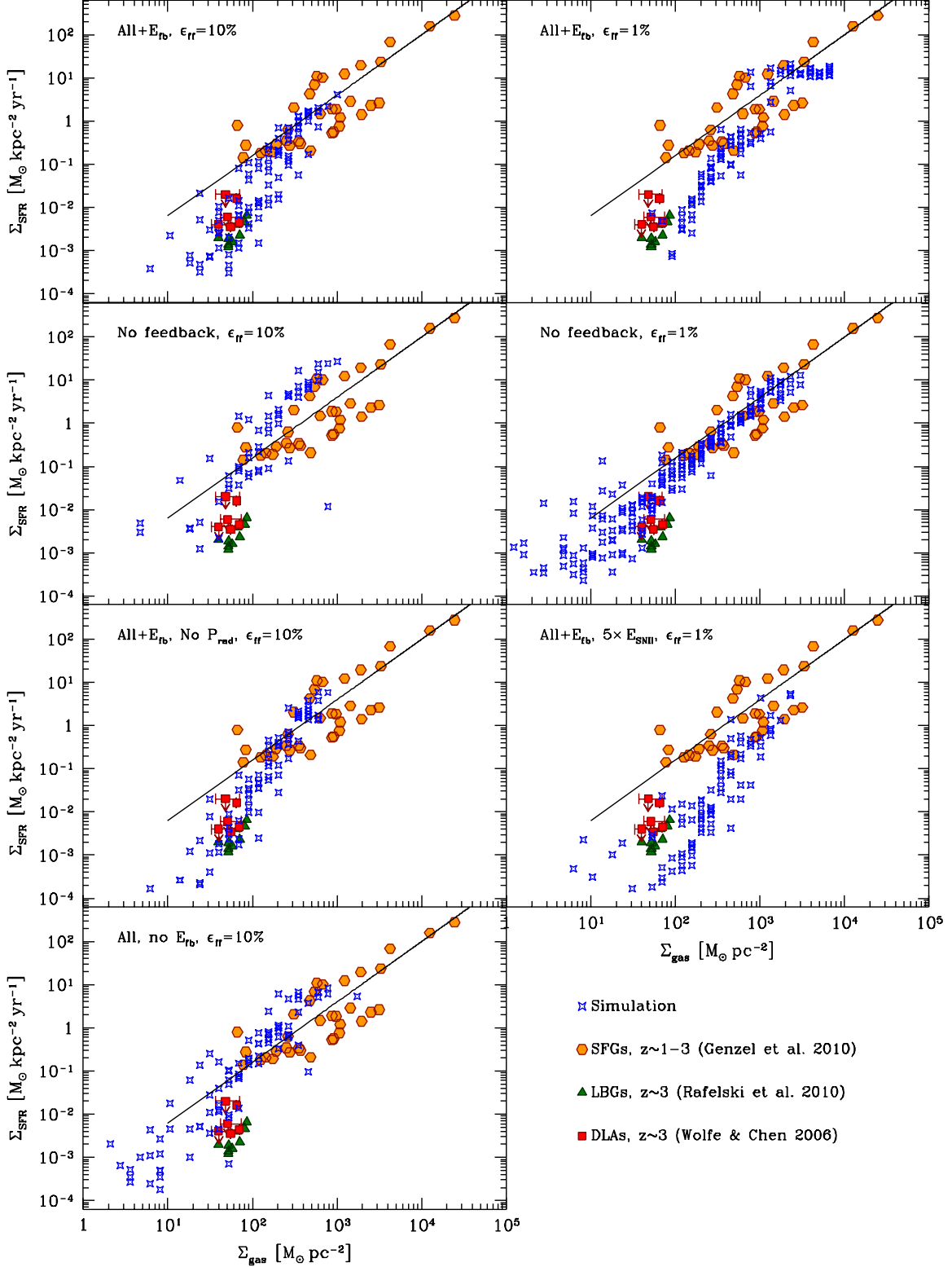


FIG. 10.— The Kennicutt-Schmidt (KS) relation ($\Sigma_{\text{gas}} - \Sigma_{\text{SFR}}$) at $z = 2 - 3$. Relation from the simulated galaxies (blue crosses) is compared to relations derived from observations: CO data for normal star forming galaxies at $z \sim 1 - 3$ (orange hexagons, Genzel et al. 2010), DLAs at $z \sim 3$ (red squares, Wolfe & Chen 2006) and LBGs at $z \sim 3$ (dark green circles, Rafelski et al. 2011). The solid black line represents the average $z = 0$ relation of Kennicutt (1998), i.e. $\Sigma_{\text{SFR}} = 2.5 \times 10^{-4} \Sigma_{\text{gas}}^{1.4} M_{\odot} \text{kpc}^{-2} \text{yr}^{-1}$. The star formation-feedback interplay establishes a wide array of relations, where the best match to observations is found for the fiducial simulation (ALL_Efb_e010) which predicts the normalization of the KS relation for $\Sigma_{\text{gas}} \gtrsim 10^2 M_{\odot} \text{pc}^{-2}$ as well as the truncation at lower surface density in agreement with the DLA/LBG observations. See main text for a discussion of the entire simulations suite.

of evolution.

Trujillo-Gomez et al. (2013), and previously Ceverino et al. (2013), presented adaptive mesh refinement (AMR) simulations of galaxy formation at high z , in the regime of dwarf galaxies ($M_{\text{halo}}(z=0) = 3 \times 10^{10} M_{\odot}$) and low mass spiral galaxies ($M_{\text{halo}}(z=0) = 2 \times 10^{11} M_{\odot}$). Using an implementation similar to what is presented in this work, the authors demonstrated the importance of considering radiation pressure in galaxy formation simulations. However, at their current resolution ($40-80 h^{-1}$ pc at $z=0$) the effect of thermal feedback is possibly underestimated, as indicated by the star formation histories in figure 8 in Trujillo-Gomez et al. (2013), where the spiral galaxy’s SFR is overpredicting the rates of Behroozi et al. (2013) by almost a dex at $z=1.5$.

Using SPH simulations of galaxy formation in halos of masses in the range $M_{\text{halo}} = 10^{11} - 3 \times 10^{12} M_{\odot}$, Aumer et al. (2013) studied the impact of their feedback model based on the multiphase SPH code presented in Scannapieco et al. (2006), with the addition of momentum input from radiation pressure. A good match to global galaxy characteristics at $z=0-4$, specifically for Milky Way analogues, were recovered if the authors considered a large value of the infrared optical depth, $\tau_{\text{IR}} = 25$, but allowed for more gentle momentum input in low redshift systems. The authors identified that despite the effort in tuning feedback parameters, the model still overpredicted the mass of stars formed at $z > 4$, and argued that this may be due to inaccurate modeling of star formation at early stages of galaxy formation or simply due to the specific merger histories of the simulated haloes.

Brook et al. (2012) and Stinson et al. (2013) discussed the importance of “early feedback” in their SPH galaxy formation simulations. These authors assume that 10% of the *bolometric* luminosity radiated by young stars get converted into thermal energy, which significantly affected properties of their simulated galaxies. Although this model differs significantly from our subgrid model of radiation pressure, in which we consider the actual momentum transfer from radiation via local gas/dust UV and IR absorption, the concept of pre-supernovae feedback was shown to have a significant effect on galaxy evolution in agreement with our conclusions.

All of the above authors have recognized the importance of additional feedback processes in addition to supernovae energy input, in particular momentum injection due to radiative feedback that pre-conditions star-forming regions before the first supernovae explosion occurs ($t \sim 4$ Myr). Recently, Marinacci et al. (2014) presented cosmological simulations, using the AREPO code (Springel 2010), of eight Milky Way-sized haloes, previously studied using dark matter only in the Aquarius project (Springel et al. 2008). The simulated galaxies had realistic sizes, rotation curves and stellar-mass to halo-mass ratios, and the authors noted this was achieved without resorting to factors thought to be crucial for galaxy formation by earlier studies, e.g. a high density threshold for star formation (e.g. Governato et al. 2010), a low star formation efficiency (Agertz et al. 2011), or early stellar feedback (e.g. Brook et al. 2012; Agertz et al. 2013; Hopkins et al. 2013). While the models of Marinacci et al. (2014) demonstrate convincing resolution convergence, as well as encouraging galaxy properties, this neither negates previous work nor comes as a surprise; Marinacci et al. adopt a stellar feedback approach based on a kinetic wind scheme in which the wind velocity, and mass loading, is scaled with the local dark matter halo size (Puchwein & Springel 2013). At the adopted

relatively low resolution ($\sim 340-680$ pc force softening), a direct modeling of strong feedback tends to affect too much gas due to mixing at the resolution scale, as well as the inability to resolve the multiphase ISM (Roškar et al. 2013). The type of wind scheme adopted by Marinacci et al. circumvents these problems by essentially postulating the existence of outflows. A natural benefit of this approach is a better resolution convergence on global galactic properties.

6.2. H_2 -based star formation and efficiency of feedback

In this work we have adopted star formation model based on the local abundance of molecular hydrogen using formalism presented by Krumholz et al. (2009a). Previous work (Gnedin et al. 2009; Gnedin & Kravtsov 2010, 2011; Kuhlen et al. 2012) have demonstrated how this approach leads to suppressed star formation in metal poor environments typical for dwarf galaxies, even resulting in a population of completely dark galaxies situated in dark matter haloes of mass $M_{\text{halo}} \lesssim 10^{10} M_{\odot}$ (Gnedin & Kravtsov 2010; Kuhlen et al. 2013). A relatively unexplored outcome of such H_2 -based star formation model is its ability to boost feedback (but see Christensen et al. 2012). In fact, in most previous studies completely neglect feedback or adopted only inefficient thermal feedback from supernovae.

Stellar feedback can be boosted in the H_2 -based star formation model in several ways. For example, star formation can become more localized because in low-metallicity environments high gas density would be required for vigorous star formation. This can lead to more correlated energy and momentum injection events. Indeed, this effect was pointed out by Christensen et al. (2012). Furthermore, as the molecular hydrogen fraction, f_{H_2} , is a function of the local dust (and hence metallicity), rapid *local* enrichment of gas from newly formed stars allows for a sudden decrease in the effective star formation threshold, leading to local burst of star formation with associated strongly correlated feedback. As we have demonstrate in this study (see Appendix A), this changes the nature of the star formation-feedback cycle, resulting in a more efficient suppression of star formation compared to models with fixed star formation density thresholds (here $n = 25 \text{ cm}^{-3}$). We note that once the numerical resolution is sufficiently high to allow for star formation to robustly occur at densities $n \gg 100 \text{ cm}^{-3}$, at which gas is expected to be mostly molecular, an explicit subgrid model for f_{H_2} may have little effect over a fixed high density threshold, as argued by Hopkins et al. (2012).

6.3. Caveats, small scale issues, and the next step

Although our simulation suite was carried with relatively high numerical resolution, most key processes related to feedback and star formation remain subgrid, as they operate on \sim pc scales within GMCs. Given that the true density probability distribution function (PDF) relevant for star formation is not fully resolved in galaxy formation simulations, the adopted star formation efficiencies per free fall time may be modified at higher resolution. The local gas depletion time is assumed to be $t_{\text{dep}} = t_{\text{ff}}/\epsilon_{\text{ff}}$, and is only modeled, and measured, on large scales ($\gtrsim 100$ pc), and the adopted value of ϵ_{ff} discussed in this work hence only applies on these scales (see Gnedin et al. 2014, for a recent discussion of how t_{dep} may manifest on different scales).

A number analytical and numerical studies of star formation in super sonic turbulence aimed at understanding

what sets the star formation efficiency per free-fall time and its evolution in GMCs has been carried out recently (see e.g. Krumholz & McKee 2005; Padoan & Nordlund 2011; Vázquez-Semadeni et al. 2011; Hennebelle & Chabrier 2011). These studies find that the value of ϵ_{ff} depends on detailed properties of star forming clouds, e.g. the flow Mach number as well as the virial parameter¹⁰, α_{vir} (see review by Padoan et al. 2013), all leading to a time dependent density PDF where stars form in the high density tail consisting of molecular clumps ($n \sim 10^2 - 10^4 \text{ cm}^{-3}$) and cores ($n \gtrsim 10^5 \text{ cm}^{-3}$). A generic result is that unless star formation is regulated by radiative feedback, protostellar outflows, subsequent supernovae as well as magnetic fields, the resulting efficiency can be significantly larger than the $\epsilon_{\text{ff}} \sim 0.25 - 0.5\%$ deduced from observations on kpc scales (see § 2.2), especially for gravitationally bound clouds ($\alpha_{\text{vir}} < 1$).

To some degree, the assumption made in our work regarding feedback regulated star formation is in line with the above results, although we apply the efficiency on much larger, $\sim 100 \text{ pc}$, scales. More work is definitely necessary in order to “connect the scales”, and future improvements in numerical resolution should allow *global* characteristic of star forming regions, such as the virial parameters α_{vir} , to be at least marginally resolved. Padoan et al. (2012) demonstrated (but see González-Samaniego et al. 2013) how the measured star formation efficiency per free fall time in high resolution simulations of supersonic turbulence could be expressed as a simple law depending only on the cloud free-fall and dynamical time, $\epsilon_{\text{ff}} \propto \exp(-1.6t_{\text{ff}}/t_{\text{dyn}})$. It remains to be seen whether this kind of assumption propagates to differences in large scale galactic observables in comparison to the choice of a large uniform ϵ_{ff} ($\sim 10\%$) in our work (see also Hopkins et al. 2013).

Furthermore, the assumption of an underlying non-linear star formation law (here $\rho_* \propto \rho_{\text{gas}}^{1.5}$) may be incorrect. Gnedin et al. (2014) argued that such as a small scale relation should result in non-linear slope in the observed KS relation which is incompatible with the linear relation observed for molecular gas ($\Sigma_{\text{SFR}} \propto \Sigma_{\text{H}_2}$) at $\Sigma_{\text{gas}} \gtrsim 100 M_{\odot} \text{ pc}^{-2}$ in the THINGS survey (Bigiel et al. 2008). Although our fiducial model is in good agreement with the observed KS relation at $z \sim 1 - 3$, it remains to be seen if the same feedback models can regulate star formation at high surface densities to be compatible with local observations of starbursts.

Finally, our stellar feedback model accounts for radiation pressure, stellar winds and supernovae type II and Ia, as well as associated max loss and metal generation where appropriate (Agertz et al. 2013). While the overall energy and momentum budget has been shown to generate realistic galaxy properties, at least for $z \gtrsim 1$, the detailed role of a separate feedback energy variable remains to be explored. It is clear that storing even a small fraction of SN energy in such variable significantly affects the star formation rate and efficacy of feedback. It is thus important to understand in detail the physical nature of such extra energy component.

As mentioned in § 2.4, this variable can be viewed as accounting for the effective pressure from a multiphase medium, where local unresolved pockets of hot gas exert work on the surrounding cold phase. Alternatively, it can be interpreted as crudely modeling kinetic energy stored in unresolved small-scale turbulence or in cosmic rays (CRs). Indeed, Booth et al.

(2013) (see also Hanasz et al. 2013; Salem & Bryan 2014) demonstrated that if a modest fraction of the available supernova energy ($\sim 10\%$ of 10^{51} erg) is injected as the CR energy density, galactic winds can be driven effectively and can exhibit qualitatively different properties compared to SN driven winds. In future work we will explore models in which cosmic ray feedback contribution to the stellar feedback budget is modeled explicitly in a fully cosmological setting.

7. CONCLUSIONS

In this paper we have presented a suite of high resolution cosmological zoom-in simulations of galaxy formation focusing on high-redshift progenitors of the Milky Way-sized galaxy forming in dark matter halo of mass $M_{200} \approx 10^{12} M_{\odot}$ at $z = 0$. We have focused on exploring how variations in the modeled star formation and feedback physics affect galaxy evolution and how properties of the simulated MW progenitors compare to modern high redshift ($z \gtrsim 1$) estimates of global characteristics, such as star formation histories, the mass-metallicity relation, the Kennicutt-Schmidt relation and the stellar mass - halo mass relation. Our simulations adopt the feedback model presented recently by Agertz et al. (2013), which accounts for energy and momentum injection via radiation pressure, stellar winds and supernovae type II and Ia. Furthermore, star formation is modeled using the local density of molecular gas (Krumholz et al. 2009a; Gnedin et al. 2009; Kuhlen et al. 2012). Our results can be summarized as follows.

- At the peak spatial resolution of our simulations, $\Delta x \sim 75 \text{ pc}$, simulated galaxy relations are sensitive not only to the details of stellar feedback processes and their parameters, but also to the underlying star formation model and adopted efficiency of star formation.
- We find that feedback can become efficient in suppressing star formation and driving outflows only if the star formation efficiency per free fall time is sufficiently large to allow for a high degree of temporal and spatial correlation of energy and momentum injection. We confirm that in the models with efficient feedback, the star formation efficiency measured on global, kiloparsec scales self-regulates to the low value inferred from observations. In our models, feedback regulation is found to occur for an input star formation efficiency per free fall time $\epsilon_{\text{ff}} = 10\%$ coupled with efficient feedback (see Agertz et al. 2013).
- If ϵ_{ff} is low ($\sim 1\%$, for the currently resolved density field), the strength of feedback must be artificially boosted to maintain efficient star formation regulation. We show that although one can match the empirical stellar mass–halo mass relation, such simulations may be in tension with the normalization of the Kennicutt-Schmidt relation. Furthermore, in agreement with other recent studies (Agertz et al. 2011; Roškar et al. 2013), we also find that simply boosting feedback with low ϵ_{ff} to match global relations prevents the formation of a well-defined gaseous disk, even at relatively low redshifts ($z \lesssim 1$). Morphology of gaseous and stellar galactic disks may therefore serve as one of the key additional constraints on the parameters of the star formation–feedback loop.

¹⁰ the ratio of the cloud kinetic energy to gravitational potential energy

- Our simulations indicate a complex interplay between parameters of star formation and stellar feedback. If the star formation efficiency is sufficiently large to allow for feedback self-regulation, removing key feedback sources, such as radiation pressure or efficient thermal feedback, moves the galaxy off observed scaling relations, but in a complex manner.
- Encouragingly, we find that our fiducial model provides a good match to all considered observables at $z \gtrsim 1$: semi-empirically derived star formation histories, the stellar mass-gas metallicity relation and evolution, the Kennicutt-Schmidt relation, the $M_* - M_{\text{halo}}$ relation and its evolution, as well as the flat shape of rotation curves.

Our results are encouraging, as they show that a comprehensive model that satisfies a number of non-trivial observational constraints and tests is feasible. Although we have only evolved the simulation to $z \sim 0.5$, and a significant fraction of stars in the $z = 0$ thin disk is expected to form after $z \sim 1$ (van Dokkum et al. 2013), we already see the formation of thin well-defined stellar disk as the turbulent gas rich disk enters

an epoch of “disk settling” (Kassin et al. 2012) around $z \sim 1.5$ (see Fig. 9 and related text). Building upon the exploratory study presented here, we will study the $z = 0$ properties of the simulated galaxies and explore the morphology of the gaseous and stellar components in future work.

The simulations presented in this paper have been carried using the Midway cluster at the University of Chicago Research Computing Center. We would like to thank Doug Rudd for his support in running the simulations. We thank Romain Teyssier for fruitful discussions. AK would like to thank the Simons foundation and organizers and participants of the Simons symposium on Galactic Super Winds in March, 2014, for stimulating and helpful discussions that aided in preparation of this paper. AK was supported via NSF grant OCI-0904482, by NASA ATP grant NNNH12ZDA001N, and by the Kavli Institute for Cosmological Physics at the University of Chicago through grants NSF PHY-0551142 and PHY-1125897 and an endowment from the Kavli Foundation and its founder Fred Kavli.

REFERENCES

- Abadi, M. G., Navarro, J. F., Steinmetz, M., & Eke, V. R. 2003, *ApJ*, 591, 499
- Agertz, O., Kravtsov, A. V., Leitner, S. N., & Gnedin, N. Y. 2013, *ApJ*, 770, 25
- Agertz, O., Teyssier, R., & Moore, B. 2009, *MNRAS*, 397, L64
- . 2011, *MNRAS*, 410, 1391
- Asplund, M., Grevesse, N., Sauval, A. J., & Scott, P. 2009, *ARA&A*, 47, 481
- Aumer, M., White, S. D. M., Naab, T., & Scannapieco, C. 2013, *MNRAS*, 434, 3142
- Avila-Reese, V., Colín, P., González-Samaniego, A., Valenzuela, O., Firmani, C., Velázquez, H., & Ceverino, D. 2011, *ApJ*, 736, 134
- Behroozi, P. S., Wechsler, R. H., & Conroy, C. 2013, *ApJ*, 770, 57
- Benson, A. J., Bower, R. G., Frenk, C. S., Lacey, C. G., Baugh, C. M., & Cole, S. 2003, *ApJ*, 599, 38
- Bigiel, F., Leroy, A., Walter, F., Brinks, E., de Blok, W. J. G., Madore, B., & Thornley, M. D. 2008, *AJ*, 136, 2846
- Bolatto, A. D., Leroy, A. K., Rosolowsky, E., Walter, F., & Blitz, L. 2008, *ApJ*, 686, 948
- Bolatto, A. D., et al. 2011, *ApJ*, 741, 12
- Booth, C. M., Agertz, O., Kravtsov, A. V., & Gnedin, N. Y. 2013, *ApJ*, 777, L16
- Brandt, A. 1977, *Math. Comp.*, 31, 333
- Brook, C. B., Stinson, G., Gibson, B. K., Wadsley, J., & Quinn, T. 2012, *MNRAS*, 424, 1275
- Bryan, G. L., & Norman, M. L. 1998, *ApJ*, 495, 80
- Ceverino, D., Klypin, A., Klimek, E., Trujillo-Gomez, S., Churchill, C. W., Primack, J., & Dekel, A. 2013, *ArXiv e-prints*
- Chabrier, G. 2003, *PASP*, 115, 763
- Christensen, C., Governato, F., Quinn, T., Brooks, A. M., Fisher, D. B., Shen, S., McCleary, J., & Wadsley, J. 2012, *ArXiv e-prints*
- Colín, P., Avila-Reese, V., Vázquez-Semadeni, E., Valenzuela, O., & Ceverino, D. 2010, *ApJ*, 713, 535
- Conroy, C., & Wechsler, R. H. 2009, *ApJ*, 696, 620
- Conroy, C., Wechsler, R. H., & Kravtsov, A. V. 2006, *ApJ*, 647, 201
- Dekel, A., & Silk, J. 1986, *ApJ*, 303, 39
- Draine, B. T. 1978, *ApJS*, 36, 595
- Edmunds, M. G. 1990, *MNRAS*, 246, 678
- Efstathiou, G. 2000, *MNRAS*, 317, 697
- Elmegreen, D. M., & Elmegreen, B. G. 2014, *ApJ*, 781, 11
- Erb, D. K., Shapley, A. E., Pettini, M., Steidel, C. C., Reddy, N. A., & Adelberger, K. L. 2006, *ApJ*, 644, 813
- Evans, II, N. J., Heiderman, A., & Vutisalchavakul, N. 2014, *ApJ*, 782, 114
- Fall, S. M., & Efstathiou, G. 1980, *MNRAS*, 193, 189
- Feldmann, R., Gnedin, N. Y., & Kravtsov, A. V. 2012, *ApJ*, 758, 127
- Font-Ribera, A., et al. 2012, *Journal of Cosmology and Astroparticle Physics*, 11, 59
- Garnett, D. R. 2002, *ApJ*, 581, 1019
- Genzel, R., et al. 2010, *MNRAS*, 407, 2091
- Gnedin, N. Y., & Kravtsov, A. V. 2010, *ApJ*, 714, 287
- . 2011, *ApJ*, 728, 88
- Gnedin, N. Y., Tasker, E. J., & Fujimoto, Y. 2014, *ArXiv e-prints*
- Gnedin, N. Y., Tassis, K., & Kravtsov, A. V. 2009, *ApJ*, 697, 55
- González-Samaniego, A., Vázquez-Semadeni, E., González, R. F., & Kim, J. 2013, *ArXiv e-prints*
- Governato, F., Willman, B., Mayer, L., Brooks, A., Stinson, G., Valenzuela, O., Wadsley, J., & Quinn, T. 2007, *MNRAS*, 374, 1479
- Governato, F., et al. 2010, *Nature*, 463, 203
- Guedes, J., Callegari, S., Madau, P., & Mayer, L. 2011, *ApJ*, 742, 76
- Guo, Q., White, S., Li, C., & Boylan-Kolchin, M. 2010, *MNRAS*, 404, 1111
- Haardt, F., & Madau, P. 1996, *ApJ*, 461, 20
- Hanasz, M., Lesch, H., Naab, T., Gawryszczak, A., Kowalik, K., & Wóltański, D. 2013, *ApJ*, 777, L38
- Hennebelle, P., & Chabrier, G. 2011, *ApJ*, 743, L29
- Heyer, M., Krawczyk, C., Duval, J., & Jackson, J. M. 2009, *ApJ*, 699, 1092
- Hinshaw, G., et al. 2013, *ApJS*, 208, 19
- Hopkins, P. F., Keres, D., Onorbe, J., Faucher-Giguere, C.-A., Quataert, E., Murray, N., & Bullock, J. S. 2013, *MNRAS* submitted (arxiv/1311.2073)
- Hopkins, P. F., Quataert, E., & Murray, N. 2011, *MNRAS*, 417, 950
- . 2012, *MNRAS*, 421, 3488
- Hummels, C. B., & Bryan, G. L. 2012, *ApJ*, 749, 140
- Kassin, S. A., et al. 2012, *ApJ*, 758, 106
- Katz, N. 1992, *ApJ*, 391, 502
- Katz, N., Weinberg, D. H., & Hernquist, L. 1996, *ApJS*, 105, 19
- Kennicutt, Jr., R. C. 1998, *ApJ*, 498, 541
- Kewley, L. J., & Ellison, S. L. 2008, *ApJ*, 681, 1183
- Klypin, A., & Prada, F. 2009, *ApJ*, 690, 1488
- Knebe, A., Kravtsov, A. V., Gottlöber, S., & Klypin, A. A. 2000, *MNRAS*, 317, 630
- Komatsu, E., et al. 2009, *ApJS*, 180, 330
- . 2011, *ApJS*, 192, 18
- Kravtsov, A., Vikhlinin, A., & Meshcheryakov, A. 2014, *ApJ* submitted (arxiv/1401.7329)
- Kravtsov, A. V. 2003, *ApJ*, 590, L1
- Krumholz, M. R., & Gnedin, N. Y. 2011, *ApJ*, 729, 36
- Krumholz, M. R., & McKee, C. F. 2005, *ApJ*, 630, 250
- Krumholz, M. R., McKee, C. F., & Tumlinson, J. 2008, *ApJ*, 689, 865
- . 2009a, *ApJ*, 693, 216
- . 2009b, *ApJ*, 699, 850
- Krumholz, M. R., & Tan, J. C. 2007, *ApJ*, 654, 304
- Kuhlen, M., Krumholz, M. R., Madau, P., Smith, B. D., & Wise, J. 2012, *ApJ*, 749, 36
- Kuhlen, M., Madau, P., & Krumholz, M. 2013, *ArXiv e-prints*
- Lada, C. J., Lombardi, M., & Alves, J. F. 2010, *ApJ*, 724, 687
- Leitherer, C., et al. 1999, *ApJS*, 123, 3
- Leitner, S. N. 2012, *ApJ*, 745, 149
- Maiolino, R., et al. 2008, *A&A*, 488, 463
- Mandelbaum, R., Seljak, U., Kauffmann, G., Hirata, C. M., & Brinkmann, J. 2006, *MNRAS*, 368, 715
- Marinacci, F., Pakmor, R., & Springel, V. 2014, *MNRAS*, 437, 1750
- McKee, C. F., & Krumholz, M. R. 2010, *ApJ*, 709, 308
- More, S., van den Bosch, F. C., Cacciato, M., Skibba, R., Mo, H. J., & Yang, X. 2011, *MNRAS*, 410, 210
- Moster, B. P., Naab, T., & White, S. D. M. 2013, *MNRAS*, 428, 3121
- Munshi, F., et al. 2013, *ApJ*, 766, 56
- Murray, N. 2011, *ApJ*, 729, 133
- Murray, N., Ménard, B., & Thompson, T. A. 2011, *ApJ*, 735, 66
- Navarro, J. F., & White, S. D. M. 1993, *MNRAS*, 265, 271

- Okamoto, T., Eke, V. R., Frenk, C. S., & Jenkins, A. 2005, *MNRAS*, 363, 1299
- Ostriker, E. C., Stone, J. M., & Gammie, C. F. 2001, *ApJ*, 546, 980
- Padoan, P., Federrath, C., Chabrier, G., Evans, II, N. J., Johnstone, D., Jørgensen, J. K., McKee, C. F., & Nordlund, Å. 2013, *ArXiv e-prints*
- Padoan, P., Haugbølle, T., & Nordlund, Å. 2012, *ApJ*, 759, L27
- Padoan, P., & Nordlund, Å. 2011, *ApJ*, 730, 40
- Pagel, B. E. J., & Patchett, B. E. 1975, *MNRAS*, 172, 13
- Piontek, F., & Steinmetz, M. 2009, preprint (ArXiv: 0909.4167)
- Pizagno, J., et al. 2007, *AJ*, 134, 945
- Planck Collaboration et al. 2013, *ArXiv e-prints*
- Pontzen, A., et al. 2008, *MNRAS*, 390, 1349
- Prochaska, J. X., Wolfe, A. M., Howk, J. C., Gawiser, E., Bures, S. M., & Cooke, J. 2007, *ApJS*, 171, 29
- Puchwein, E., & Springel, V. 2013, *MNRAS*, 428, 2966
- Rafelski, M., Wolfe, A. M., & Chen, H.-W. 2011, *ApJ*, 736, 48
- Raiteri, C. M., Villata, M., & Navarro, J. F. 1996, *A&A*, 315, 105
- Reyes, R., Mandelbaum, R., Gunn, J. E., Nakajima, R., Seljak, U., & Hirata, C. M. 2012, *MNRAS*, 425, 2610
- Romeo, A. B., Agertz, O., Moore, B., & Stadel, J. 2008, *ApJ*, 686, 1
- Rosen, A., & Bregman, J. N. 1995, *ApJ*, 440, 634
- Rosolowsky, E., & Blitz, L. 2005, *ApJ*, 623, 826
- Roškar, R., Teyssier, R., Agertz, O., Wetzstein, M., & Moore, B. 2013, *ArXiv e-prints*
- Salem, M., & Bryan, G. L. 2014, *MNRAS*, 437, 3312
- Scannapieco, C., Tissera, P. B., White, S. D. M., & Springel, V. 2006, *MNRAS*, 371, 1125
- . 2008, *MNRAS*, 389, 1137
- Scannapieco, C., White, S. D. M., Springel, V., & Tissera, P. B. 2009, *MNRAS*, 396, 696
- Scannapieco, C., et al. 2012, *MNRAS*, 423, 1726
- Schaye, J. 2001, *ApJ*, 562, L95
- Silk, J., & Mamon, G. A. 2012, *Research in Astronomy and Astrophysics*, 12, 917
- Silk, J., & Rees, M. J. 1998, *A&A*, 331, L1
- Springel, V. 2010, *MNRAS*, 401, 791
- Springel, V., Frenk, C. S., & White, S. D. M. 2006, *Nature*, 440, 1137
- Springel, V., et al. 2008, *MNRAS*, 391, 1685
- Stinson, G., Seth, A., Katz, N., Wadsley, J., Governato, F., & Quinn, T. 2006, *MNRAS*, 373, 1074
- Stinson, G. S., Brook, C., Macciò, A. V., Wadsley, J., Quinn, T. R., & Couchman, H. M. P. 2013, *MNRAS*, 428, 129
- Sutherland, R. S., & Dopita, M. A. 1993, *ApJS*, 88, 253
- Tassis, K., Kravtsov, A. V., & Gnedin, N. Y. 2008, *ApJ*, 672, 888
- Teyssier, R. 2002, *A&A*, 385, 337
- Teyssier, R., Pontzen, A., Dubois, Y., & Read, J. I. 2013, *MNRAS*, 429, 3068
- Thacker, R. J., & Couchman, H. M. P. 2001, *ApJ*, 555, L17
- Tremonti, C. A., et al. 2004, *ApJ*, 613, 898
- Trujillo-Gomez, S., Klypin, A., Colin, P., Ceverino, D., Arraki, K., & Primack, J. 2013, *ArXiv e-prints*
- Tully, R. B., & Fisher, J. R. 1977, *A&A*, 54, 661
- van Dokkum, P. G., et al. 2013, *ApJ*, 771, L35
- Vázquez-Semadeni, E., Banerjee, R., Gómez, G. C., Hennebelle, P., Duffin, D., & Klessen, R. S. 2011, *MNRAS*, 414, 2511
- Vikhlinin, A., et al. 2009, *ApJ*, 692, 1060
- Weinmann, S. M., Pasquali, A., Oppenheimer, B. D., Finlator, K., Mendel, J. T., Crain, R. A., & Macciò, A. V. 2012, *MNRAS*, 426, 2797
- White, S. D. M., & Rees, M. J. 1978, *MNRAS*, 183, 341
- Wise, J. H., Turk, M. J., Norman, M. L., & Abel, T. 2012, *ApJ*, 745, 50
- Wolfe, A. M., & Chen, H. 2006, *ApJ*, 652, 981
- Wolfire, M. G., Tielens, A. G. G. M., Hollenbach, D., & Kaufman, M. J. 2008, *ApJ*, 680, 384

APPENDIX

A. IMPACT OF A FIXED DENSITY THRESHOLD FOR STAR FORMATION

The assumed star formation model throughout the is work is based on the abundance of molecular hydrogen, see Eq. 1. A more common approach in the galaxy formation community is to only allow stars to form above some fixed density threshold ρ_* , i.e.

$$\dot{\rho}_* = \frac{\rho_g}{t_{\text{SF}}} \text{ for } \rho > \rho_*. \quad (\text{A1})$$

The appropriate value of this threshold is highly resolution dependent, as galaxy formation simulations do not yet converge on a density PDF representative of the ISM, and values of this threshold greatly vary in the literature (see discussion in Agertz et al. 2011). To study the impact of the star formation prescription choice, we adopt the density threshold of $\rho_* = 25 \text{ cm}^{-3}$, which roughly corresponds to the physical density at which $f_{\text{H}_2} \sim 50\%$ at $Z_g = Z_\odot$ (Gnedin et al. 2009). Fig. 11 shows dependence of the star formation history of the main progenitor on changes of the star formation prescription *only*, from the molecular based prescription adopted in our study to the fixed density threshold prescription of Eq. A1. All the other feedback and star formation related settings, e.g. the efficiency per-free-fall were fixed at their fiducial values. The H_2 model results in SFRs lower by ~ 0.5 dex for $z < 7$ compared to the traditional constant density threshold model. The latter disagrees with the Behroozi et al inference at all redshifts. As shown in the figure, the constant threshold model is in fairly good agreement with the SFH of the Eris simulation (Guedes et al. 2011), which also adopted the constant threshold based star formation model, but with the threshold of $n_* = 5 \text{ cm}^{-3}$. Note that the virial mass of the Eris simulation ($M_{\text{vir}} \approx 7.9 \times 10^{11} M_\odot$) is $\sim 20\%$ lower than the simulated halo in this study.

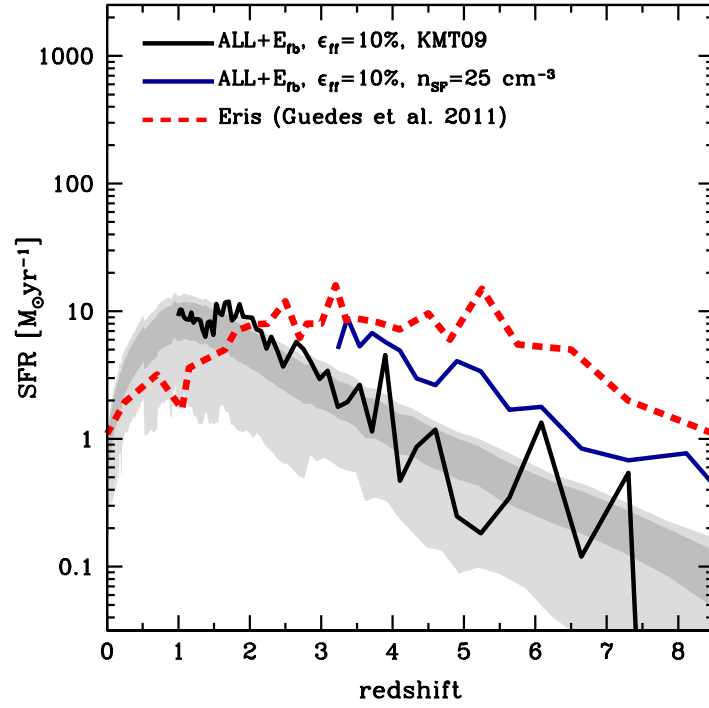


FIG. 11.— Simulated star formation histories compared to the Behroozi et al. (2013) data for $M_{\text{vir}}(z=0) = 10^{12} M_{\odot}$. Dark and light gray shaded areas are one- and two-sigma confidence regions respectively. We adopt bins of size $\Delta t_{\text{SF}} = 100 \text{ Myr}$ for the simulated SFHs. The KMT09 model shows SFRs lower by ~ 0.5 dex compared to the fixed density threshold model. For comparison we also plot the SFH of the Eris simulation (Guedes et al. 2011).